DEBONDING OF EXTERNALLY BONDED POLYPARA PHENYLENE BENZOBISOXAZOLE
(PBO) MESHES FOR FLEXURAL STRENGTHENING OF REINFORCED CONCRETE BEAMS

Mr. Chanh Thai Minh Tran

A Dissertation Submitted in Partial Fulfillment of the Requirements

for the Degree of Doctor of Philosophy Program in Civil Engineering

Department of Civil Engineering

Faculty of Engineering

Chulalongkorn University

Academic Year 2014

การหลุดลอกของแผ่นโพลิเมอร์เสริมเส้นใย POLYPARA PHENYLENE BENZOBISOXAZOLE
(PBO)ที่ใช้ติดผิวนอกของคานคอนกรีตเสริมเหล็กเพื่อเสริมกำลังดัด

นายชาน ไทย มิน ทราน

Thesis Title	DEBONDING OF EXTERNALLY BONDED POLYPARA PHENYLENE BENZOBISOXAZOLE (PBO) MESHES FOR FLEXURAL STRENGTHENING OF REINFORCED CONCRETE BEAMS
By	Mr. Chanh Thai Minh Tran
Field of Study	Civil Engineering
Thesis Advisor	Associate Professor Boonchai Stitmannaithum, D.Eng.
Thesis Co-Advisor	Professor Ueda Tamon, D.Eng.

Accepted by the Faculty of Engineering, Chulalongkorn University in Partial Fulfillment of the Requirements for the Doctoral Degree

---Dean of the Faculty of Engineering

(Professor Bundhit Eua-arporn, Ph.D.)

THESIS COMMITTEE

---Chairman

(Professor Thaksin Thepchatri, Ph.D.)

---Thesis Advisor

(Associate Professor Boonchai Stitmannaithum, D.Eng.)

---Thesis Co-Advisor

(Professor Ueda Tamon, D.Eng.)

---Examiner

(Associate Professor Akhrawat Lenwari, Ph.D.)

---Examiner

(Assistant Professor Withit Pansuk, Ph.D.)

---External Examiner

(Raktipong Sahamitmngkol, Ph.D.)

ชาน ไทย มิน ทราน : การหลุดลอกของแผ่นโพลิเมอร์เสริมเส้นใย POLYPARA PHENYLENE BENZOBISOXAZOLE (PBO)ที่ใช้ติดผิวนอกของคานคอนกรีตเสริมเหล็กเพื่อเสริมกำลังดัด (DEBONDING OF EXTERNALLY BONDED POLYPARA PHENYLENE BENZOBISOXAZOLE (PBO) MESHES FOR FLEXURAL STRENGTHENING OF REINFORCED CONCRETE BEAMS) อ.ที่ปรึกษาวิทยานิพนธ์หลัก: รศ. ดร.บุญไชย สถิตมั่นในธรรม, อ.ที่ปรึกษาวิทยานิพนธ์ร่วม: ศ. ดร.อูเอดะ ทามอน, หน้า.

ในปัจจุบันมีโครงสร้างคอนกรีตจำนวนมากที่ไม่บรรลุตามข้อกำหนดที่ใช้ในการออกแบบและอายุการใช้งานทั้งนี้เนื่องจากโครงสร้างเผชิญกับการเสื่อมสภาพ เช่น ปัจจัยเวลา การบรรทุกน้ำหนักเกิน และการกัดกร่อน ดังนั้นจึงมีความจำเป็นที่จะต้องมีการบำรุงรักษา ซ่อมแซม และเสริมกำลังโครงสร้างเพื่อยืดอายุการใช้งาน โดยวิธีการในการบำรุงรักษา ซ่อมแซม และเสริมกำลังโครงสร้างได้ถูกนำเสนอหลายวิธีในช่วงทศวรรษที่ผ่านมาจากทั้งประสบการณ์ตรงจากการทำงานและจากนักวิจัย การใช้ระบบแผ่นโพลิเมอร์เสริมเส้นใย (Fiber reinforced polymer, FRP) ซึ่งทำจากแผ่นโพลิเมอร์เสริมเส้นใยและอีพ็อกซี่เรซิ่น (epoxy resin) เป็นหนึ่งในวิธีที่ได้รับการยอมรับแพร่หลายในด้านการเพิ่มกำลังรับแรงของชิ้นส่วนโครงสร้างคอนกรีตเสริมเหล็ก ทั้งนี้เนื่องจากคุณสมบัติที่ดีของวัสดุ เช่น มีอัตราส่วนความแข็งแรงต่อน้ำหนักสูงและความสามารถในการความต้านทานการกัดกร่อน อย่างไรก็ตามระบบ FRP ยังมีข้อเสียเปรียบ เนื่องจากจำเป็นที่จะต้องใช้อีพ็อกซี่เรซิ่น ซึ่งเป็นสารเชื่อมประสานที่มีความทึบน้ำต่ำ ความทนไฟต่ำ ไม่สามารถใช้บนพื้นผิวชื้นได้ และไวต่อรังสียูวี

เพื่อที่จะไม่เกิดปัญหาที่กล่าวมาข้างต้น ระบบมอร์ต้าซีเมนต์เสริมเส้นใย (Fiber reinforced cementitious mortar, FRCM) ได้ถูกนำเสนอขึ้น ระบบ FRCM ประกอบด้วยตาข่ายเส้นใยฝังลงในซีเมนต์ ซึ่งเป็นระบบที่มีคุณสมบัติเชิงกลที่ดี มีความทนไฟสูง และมีความทึบน้ำสูง นอกจากนี้ยังสามารถใช้ได้ในพื้นผิวเปียก ดังนั้นระบบ FRCM จึงเป็นทางเลือกหนึ่งของระบบ FRP สำหรับการเสริมกำลังและซ่อมแซมโครงสร้างคอนกรีต นวัตกรรมการเสริมกำลังด้วยแผ่นโพลิเมอร์เสริมเส้นใย Polypara phenylene benzobisoxazole (PBO) ซึ่งฝังอยู่ในซีเมนต์และคอนกรีตสำหรับการติดที่ผิวนอกเพื่อเสริมกำลังโครงสร้างคอนกรีตเสริมเหล็กถือเป็นหนึ่งในเทคโนโลยีที่น่าสนใจสำหรับวิศวกรโครงสร้าง

พฤติกรรมการหลุดลอกเป็นลักษณะสำคัญที่ใช้ประเมินประสิทธิผลของระบบการเสริมกำลังใดๆ ซึ่งพฤติกรรมการหลุดลอกขึ้นอยู่กับกลไกการส่งถ่ายแรงระหว่าง FRCM และผิวคอนกรีตของโครงสร้าง อย่างไรก็ตามจางจากการทบทวนงานวิจัยพบว่าการศึกษาเกี่ยวกับพฤติกรรมการหลุดลอกของ PBO-FRCM ที่ใช้ติดผิวนอกของคานคอนกรีตเสริมเหล็กเพื่อเสริมกำลังยังมีน้อย ดังนั้นในงานวิจัยนี้จึงมุ่งศึกษาพฤติกรรมการหลุดลอก PBO-FRCM ที่ใช้ติดผิวนอกของคานคอนกรีตเสริมเหล็กภายใต้การทดสอบแรงดัดแบบสี่จุด (four-point flexure tests)

งานวิจัยนี้ประกอบด้วยส่วนการทดลองและการวิเคราะห์ของการใช้ PBO-FRCM เพื่อเสริมกำลังคานคอนกรีตเสริมเหล็ก วัตถุประสงค์ของงานวิจัยนี้คือ (1) หาระยะยึดเหนี่ยวประสิทธิผลของ PBO mesh ที่ใช้ในระบบ PBO-FRCM (2) หากฎความสัมพันธ์ของแรงยึดเหนี่ยวและการเลื่อนไถลระหว่าง PBO mesh และคอนกรีต (3) ศึกษาพฤติกรรมของรอยแตกที่เหนี่ยวนำให้เกิดการหลุดลอก (IC debonding) ของการเสริมกำลังด้วย PBO-FRCM ภายใต้แรงดัด (4) เสนอแบบจำลองเพื่อทำนาย IC debonding สำหรับคานที่เสริมกำลังดัดด้วย PBO-FRCM

การศึกษานี้แบ่งออกเป็นสองส่วน ส่วนที่หนึ่งคือส่วนที่ได้จากการทดลอง และส่วนที่สองคือผลจากการวิเคราะห์ โดยส่วนแรกสามารถแบ่งได้เป็น 2 ระยะ ระยะที่หนึ่งคือการทดสอบแรงฉือนของ 12 ชิ้นตัวอย่างเพื่อหาค่าระยะยึดเหนี่ยวประสิทธิผล และระยะที่สองเป็นการทดลองเพื่อหากฎความสัมพันธ์ของแรงยึดเหนี่ยวและการเลื่อนไถล ประกอบด้วยชิ้นตัวอย่างจำนวน 9 ตัวอย่าง ในส่วนที่ 2 (ส่วนการวิเคราะห์)ประกอบด้วย 2 ระยะ ระยะที่หนึ่งคือการพัฒนาแบบจำลองสำหรับการวิเคราะห์เพื่อหาค่ากฎความสัมพันธ์ของแรงยึดเหนี่ยวและการเลื่อนไถลระหว่าง PBO mesh และคอนกรีต และระยะที่สองคือการวิเคราะห์และทำนายพฤติกรรมการรับแรงดัดของคานคอนกรีตเสริมเหล็กที่เสริมกำลังด้วยระบบ PBO-FRCM ประสิทธิภาพและความแม่นยำของแบบจำลองได้รับการตรวจสอบโดยเปรียบเทียบกับผลจากการทดลอง ผลจากการทดลองยังใช้เพื่อหาผลกระทบของตัวแปรที่แตกต่างกัน ผลการทดลองเป็นในรูปของค่าการโก่งตัว ความเครียดในวัสดุและรูปแบบการวิบัติ จากผลการทดลองและการวิเคราะห์ในงานวิจัยนี้นำไปสู่ข้อสรุปและข้อเสนอแนะสำหรับคานคอนกรีตเสริมเหล็กที่เสริมกำลังด้วยระบบ PBO-FRCM

ภาควิชา   วิศวกรรมโยธา   ลายมือชื่อนิสิต _____
สาขาวิชา   วิศวกรรมโยธา   ลายมือชื่อ อ.ที่ปรึกษาหลัก _____
ปีการศึกษา   2557   ลายมือชื่อ อ.ที่ปรึกษาร่วม _____

5371843021 : MAJOR CIVIL ENGINEERING

KEYWORDS:

CHANH THAI MINH TRAN: DEBONDING OF EXTERNALLY BONDED POLYPARA PHENYLENE BENZOBISOXAZOLE (PBO) MESHES FOR FLEXURAL STRENGTHENING OF REINFORCED CONCRETE BEAMS. ADVISOR: ASSOC. PROF. BOONCHAI STITMANNAITHUM, D.Eng., CO-ADVISOR: PROF. UEDA TAMON, D.Eng., pp.

Nowadays, there are a lot of existing concrete structures that do not satisfy design and lifetime requirements due to suffering from many adverse conditions such as aging, overload and corrosion. Maintaining, repairing, strengthening and retrofitting for these structures are necessary to extend their lifetime. Several techniques based on practical experiences and scientific researches have been proposed during recent decades. Among these techniques, fiber reinforced polymer (FRP) strengthening systems made of fiber sheets and epoxy resin have been widely accepted to increase the load-carrying capacity of reinforced concrete (RC) structural members because of their favorable properties, such as high strength-to-weight ratio and corrosion resistance. However, there are some drawbacks of FRP systems that are unavoidable due to the usage of epoxy resin. In fact the epoxy bond agent has low permeability, poor fire resistance, is impossible to apply on humid surfaces and is susceptible to UV radiation.

To overcome some of these obstacles, fiber reinforced cementitious mortar (FRCM) systems made of fiber meshes embedded in a cementitious matrix have been proposed. These materials of the FRCM systems have good mechanical performance, high resistance to temperature and fire, and have good vapor permeability. They can be applied on wet surfaces. Therefore, the FRCM systems have become an alternative option to the FRP systems for strengthening and repairing RC structures. The innovative strengthening system made of polypara phenylene benzobisoxazole (PBO) fiber mesh embedded in cementitious matrix and concrete recently for external strengthening of RC structures has emerged as one of the most exciting and promising technologies in material and structural engineering.

Debonding phenomenon is an important characteristic to evaluate the effectiveness of any strengthening systems and it strongly depends on the transfer load mechanism at the FRCM strengthening material and concrete substrate interface. Until now, very few studies have investigated on the debonding phenomena in RC beam strengthened with PBO-FRCM system. So that, we continue to investigate on the debonding behavior of PBO-FRCM strengthening RC beams under four-point flexure tests in this study. My research included both experimental work and analytical work on the use of PBO-FRCM for strengthening RC beams. The main objectives of my research are: (1) the effective bond length of PBO mesh for PBO-FRCM system, (2) the bond slip law between PBO mesh and concrete, (3) the intermediate crack induced debonding (IC debonding) behavior of PBO-FRCM strengthened RC beams under bending load, and (4) proposed model for predicting IC debonding for beams strengthened with PBO-FRCM under flexural condition.

To achieve these objectives, this study was divided into two parts. The first part showed the experimental work while the second part presented the analytical work. There were two phases in first part. The first phase included the shear test of 12 specimens for determining effective bond length. And the second phase included 9 specimens for investigating bond slip law. There were also two phases in second part. The first phase included developing an analytical model to obtain bond slip law between PBO materials and concrete, and the second phase included analyzing and predicting the behavior of RC beams strengthened with PBO-FRCM systems in flexure load. The efficiency and accuracy of these models were verified by comparing their results to the experimental results. The experimental work was also used to investigate the effects of different parameters. The tested results are showed in terms of deflections, strains in materials and failure modes. Based on the experimental and analytical work, useful conclusions and recommendations for beams strengthened with PBO-FRCM system were provided.

Department: Civil Engineering	Student's Signature	--
Field of Study: Civil Engineering	Advisor's Signature	--
Academic Year: 2014	Co-Advisor's Signature	--

ACKNOWLEDGEMENTS

CONTENTS

LIST OF FIGURES

LIST OF TABLES

Chapter 1

Introduction

1.1 General

In many developed countries, there are a lot of existing reinforced concrete infrastructures that do not satisfy the design and lifetime requirements due to suffering many adverse conditions such as environmental effects and improper use or maintenance of these structures. These are a law of nature that the most modern structures are affected. Therefore, there has been a high challenge for engineers to find out the satisfactory methods for solving the failure problems of these infrastructures. To extend their lifetime, structures may be maintained, repaired and retrofitted to satisfy load capacity, durability and reliability of structures. Several techniques based on practical experience and scientific research are proposed during recent decades. Among these techniques, fiber reinforced polymer (FRP) strengthening systems made of fiber sheet and epoxy resin have been widely accepted to increase the load-carrying capacity of reinforced concrete (RC) structural members due to their favorable properties, such as high strength to weight ratio and corrosion resistance. However, there are some drawbacks of FRP systems that are unavoidable due to usage of epoxy resin. Actually, epoxy bond agent has low permeability, poor fire resistance, impossible application on humid surface and susceptibility to UV radiation

To overcome some of these obstacles, innovative fiber reinforced cementitious mortar (FRCM) systems made of fiber mesh embedded in cementitious mortar have been proposed. These materials have good mechanical performance, high resistance against temperature and fire, and good vapor permeability, and they can be applied on wet surfaces. Therefore, FRCM strengthening systems have become an alternative option to FRP systems in term of strengthening and repairing RC structures. The FRCM strengthening system made of polypara phenylene benzobisoxazole (PBO) fiber mesh embedded in cementitious matrix and concrete recently for external strengthening of RC structures has emerged as one of the most exciting and promising technologies in material and structural engineering.

There are many strengthening systems based cement matrix for RC structures in technical literature such as the textile reinforced concrete (TRC) (A. Bruckner 2005), the textile reinforced mortar (TRM) (Triantafillou and Papanicolaou 2006), the fiber reinforced concrete (FRC) (Wu and J.Teng 2002, Wu and Sun 2005), the mineral based composites (MBC) (Taljsten and Blanksvard 2007, 2008) and the fiber reinforced cementitious mortar (FRCM) (Bisby et al. 2011, Ombres 2011a, 2011b, D'Ambrisi et al. 2012a, 2012b, 2013). The TRC is made of multi-axial textile fabrics and concrete with a fine-grained, high strength concrete. The TRM system consists of textile fabrics and concrete with polymer modified mortar as a bond agent. The FRC is made of fibers impregnated with a cement matrix and concrete. The MBC is made of fiber

composite gird and concrete with cementitious binder. And the FRCM system is made of fiber mesh embedded in cementitious mortar and concrete.

PBO-FRCM strengthening material for RC structures is still under investigation. The effectiveness of this new strengthening system was evidenced by some previous research (Tommaso et al. 2007, Tommaso et al. 2008, Ombres 2009, 2011a) in terms of strength and ductility. However, previous experimental results also showed that IC debonding was the main failure that occurred in beams with PBO-FRCM systems. And, as we known, debonding phenomenon is an important characteristic to evaluate the effectiveness of any strengthening system and strongly depended on the transfer load mechanisms at the concrete/matrix interface. Because the transfer load mechanism of PBO-FRCM system is different from that of FRP system, so that the debonding process in PBO-FRCM strengthened RC beams is different than that observed in FRP strengthened RC beams. In fact, the debonding phenomena occur in the concrete substrate in case of FPR systems and the debonding phenomena occur within the cementitious matrix with in case of PBO-FRCM.

In addition, predictions of debonding models of FRP strengthened RC beams are not accurate to apply for PBO-FRCM strengthened system when debonding failures occur. Difference between predictions and experimental values, observed in terms both of ultimate capacity and debonding strains were, in fact, in the range 3-40% (Ombres 2011b). Therefore, in this research we continue to investigate on the debonding

behavior of beams strengthened with PBO-FRCM system under four-point flexural test.

1.2 Research objective

The consequence of debonding failure of strengthened beam with externally strengthening system is usually sudden and catastrophic. And it will affect directly on the effectiveness of strengthening system. Since at present, very few studies have investigated on the debonding phenomena in strengthened beams with PBO-FRCM system and there are not any available bond-slip laws between PBO-FRCM and concrete to take into account the transfer load mechanism at the interface between PBO-FRCM and concrete. Therefore, the main objectives of this study conducted at the Chulalongkorn University, Department of Civil Engineering are:

- To determine the effective bond length of PBO mesh for PBO-FRCM system.

- To establish and develop the bond-slip relationship between PBO-FRCM and concrete.

- To investigate the IC debonding behavior of strengthened beams with PBO-FRCM system under bending test

- To propose a model for predicting IC debonding for beams strengthened with PBO-FRCM system under flexure load.

1.3 Methodology

To achieve above objectives, both experiment work and analysis work are conducted in this study as shown in Figure 1. The experimental work includes two phase: (1) shear test and (2) bending test. And the analytical work also includes two phase: (1) model of bond stress-slip between PBO-FRCM and concrete and (2) model for predicting debonding of beams strengthened with PBO-FRCM system.
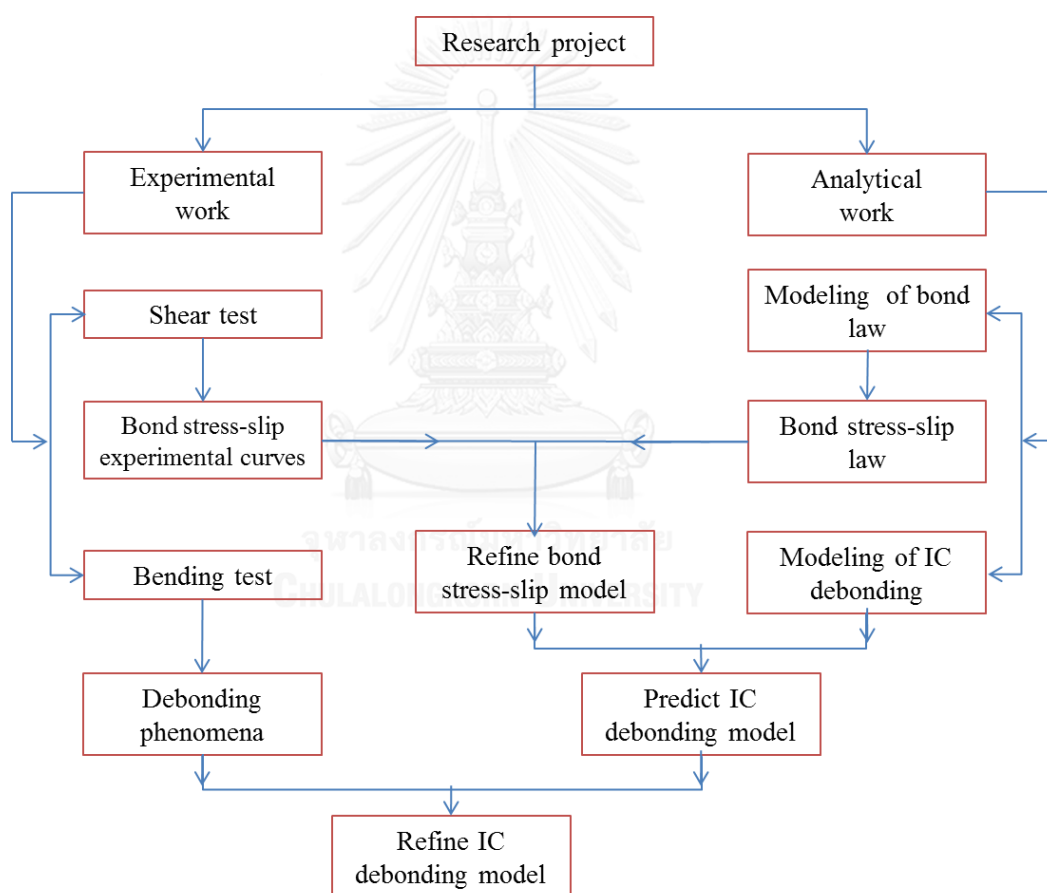
Figure 1. 1 Research methodology

1.4 Thesis structure

This dissertation is divided into six chapters as shown in Figure 1.2

Chapter 1 provides the Introduction to PBO-FRCM strengthening system, research objectives, methodology to achieve the research objectives and the organization of thesis

Chapter 2 presents the literature review including properties of PBO material, application field of PBO and research about PBO-FRCM strengthening systems

Chapter 3 describes the experimental program, fabrication of tested specimens, strengthening procedures, instrumentation and test set-up

Chapter 4 presents the experimental result and discussion included effective bond length of PBO and bond stress-slip relationship. Proposed model for bond stress-slip between PBO and concrete are also discussed.

Chapter 5 presents the experimental results and discussion of bending test. A proposed model for predict IC debonding of beams strengthened with PBO-FRMC also is described.

Chapter 6 shows the conclusions and recommendations for future work.
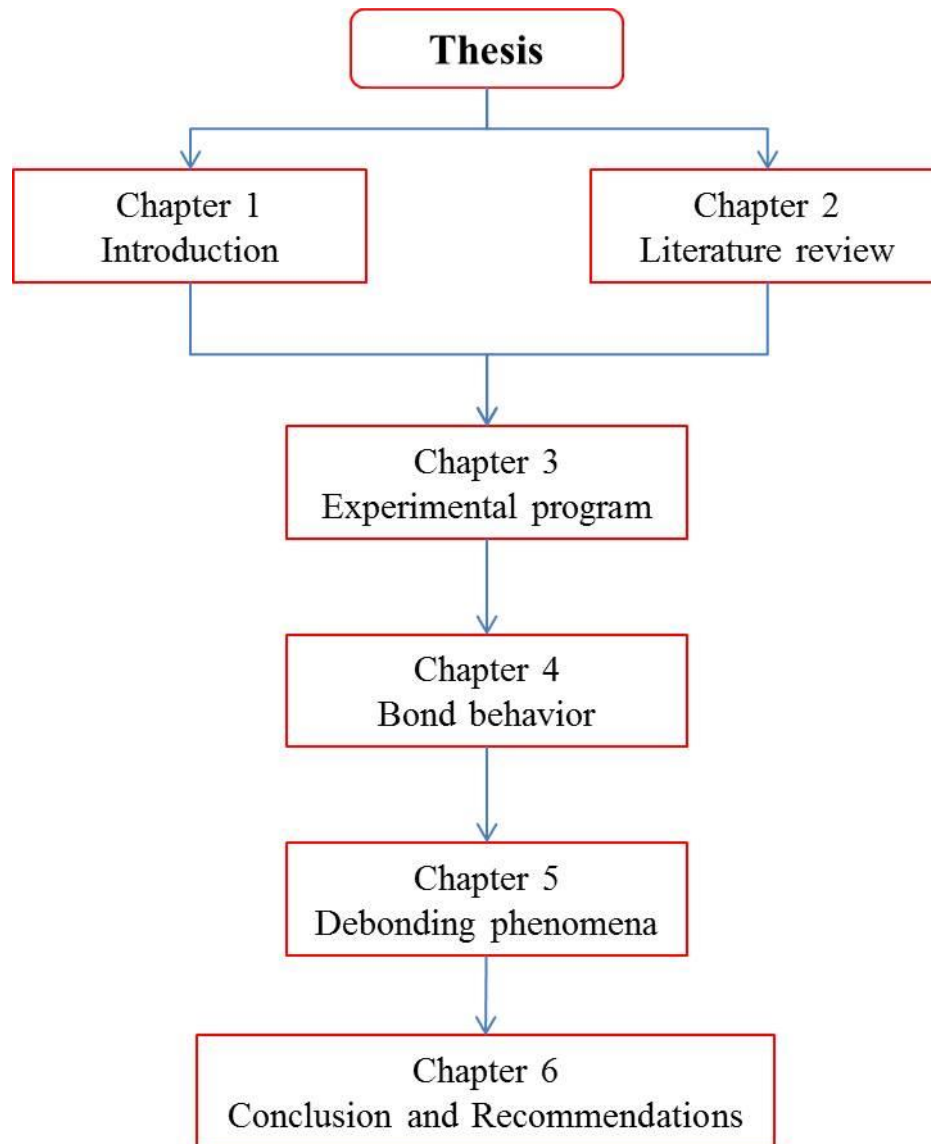
Figure 1. 2 Thesis layout

Chapter 2

Literature review

2.1   General

PBO fibers represent the new generation of super fibers with ultra-high resistance and

high tensile strength. The properties of PBO fiber are reported in Table 1.

Table 2. 1 The properties of PBO fiber [6]

Density (g/cm^3)	1.56
Tensile strength (GPa)	5.8
Modulus of elasticity (GPa)	270
Ultimate elongation (%)	2.1
Decomposition temperature (^{o}C)	650
Thermal dilation coefficient ($10^{-6}\,^o$C^{-1})	-6

In comparison with other fibers (Ruredil 2006), the properties of PBO fiber has the

highest tensile strength and modulus as reported in Table 2.

Table 2. 2 Comparison of mechanical properties with other types of fiber

Type of fiber	Tensile strength (MPa)	Modulus of elasticity (GPa)	Ultimate deformation (%)	Density (g/cm^3)	Resistance to heat ($^{\circ}$C)	Coefficient of thermal dilation ($10^{-6}\,^{\circ}C^{-1}$)
PBO	5800	270	2.5	1.56	650	-6
Carbon (high strength)	4100	240	1.6	1.75	1400	-1.45
Aramid (high modulus)	2800	109	2.4	1.45	550	-2
Aramid	650	17	2.2	1.38	400	-2
Construction steel	250-400 (yield) 300-600 (breakage)	206	20-30	7.8	--	+10.4
Glass	3500	80	4.5	2.5	1200	+5.4

2.2   Applications of PBO fiber

PBO-FRCM strengthening material has the same performance as conventional FRP techniques, so that it may be used to strengthen and repair for concrete and masonry structures including those which can be subject to the simultaneous action of high temperature.

Due to advantages of PBO fiber, it can be used in following applications:

- Flexural reinforcement

- Shearing reinforcement

- Torsion reinforcement

- Seismic retrofitting

2.3   Researches of FRCM strengthening systems

2.3.1 General

Some studies have been investigation on the behavior of concrete structures with strengthening systems based on cement matrix and their results are available in the technical literature. The RC beams strengthened with carbon fiber sheets bonded with inorganic (low viscosity resin) and organic (epoxy resin) matrixes were conducted by Toutanji (Toutanji et al. 2006, Toutanji and Deng 2007) in bending test. The experimental results showed that the inorganic matrix system was as effective in increasing strength and stiffness of RC beams as the organic matrix system. And the load transfer mechanism in case of inorganic strengthening systems was different from that of organic strengthening systems. Many micro cracks occurred and the failure modes were fracture of the carbon fiber sheets for RC beams strengthened with inorganic strengthening systems while the failure modes were delamination for RC beams strengthened with organic strengthening systems. The tested results also showed that the failure modes of beams depended on the amount of FRP and transferred from FRP rupture to delamination of FRP from the concrete substrate.

The effectiveness of the TRC systems were conducted and analyzed by Bruckner (A. Bruckner 2005). RC slabs strengthened in bending and RC beams strengthened in shear were tested. The tested results investigated if TRC strengthening systems

increased both the load carrying capacity and the shear load capacity of RC elements.

The RC beams strengthened with TRM strengthening systems were investigated by Triantafillou and Papanicolaou (2006). The tested results showed that the TRM strengthening systems increased the shear load capacity of RC beams.

The behavior of RC elements strengthened with the FRC strengthening systems were conducted by Wu (Wu and J.Teng 2002, Wu and Sun 2005). The FRC strengthening systems were made of fibers impregnated with a cement matrix and concrete. The results of tested concrete beams and cylinders strengthened with both carbon FRC (CFRC) and carbon FRP (CFRP) evidenced that there were significantly increased both flexural capacity and compressive strength of concrete by using FRC wraps. The ductility of the strengthened concrete also increased significantly. The confined concrete cylinders were failed by rupture of composite wrap and the tested beams were failed by rupture of the FRC sheet.

The effectiveness of the MBC strengthening system was investigated by Taljsten and Blanksvard (2007). The RC slabs strengthened with CFRP girds and bonded to concrete both with cementitious and epoxy bonding agent in flexure strengthening were carried out. The tested results showed that the slabs strengthened with cementitious bonding agent are comparable to the slabs strengthened with epoxy

bonding agent. The failure mode for the slab strengthened with sanded CFRP gird and epoxy was brittle while the failure mode of other specimens was ductile.

A new FRCM system made of fiber meshes embedded in cementitious has been proposed recently. These materials of FRCM system have good mechanical performance, high resistance against high temperature and fire, and good vapor permeability and capable applying on wet surfaces. The transfer load mechanism and characteristics of FRCM strengthening systems are still under investigation.

2.3.2 Bond stress-slip relationship between FRCM strengthening system and concrete

The bond between the strengthening material and concrete is the key role for the effectiveness of any strengthening systems. It was different and depended on the characteristic of each strengthening system. In fact, debonding phenomena occurred within cementitious matrix or at the fiber and cementitious matrix interface in case of FRCM systems, while debonding phenomena occurred within concrete substrate or epoxy matrix and concrete interface in case of FRP system (D'Ambrisi et al. 2012a, 2012b).

Experimental results of bond tests on a C-FRCM system for the external strengthening of masonry elements had been conducted (D'Ambrisi et al. 2013). The results showed that the debonding mechanism essentially consisted of the gradual

loss of bond at the fibers and cementitious matrix interface. And the effective anchorage length was lower than 110 mm.

The bond stress transfer between PBO mesh and concrete had been investigated by D'Ambrisi et al. (2012b) recently. In case of one layer, bond length L of 50, 100, 150 and 250 mm were adopted. And in case of two layers, bond length L of 100 and 200 mm were adopted. The experimental analysis investigated if: the debonding phenomena occurred at the fibers and cementitious matrix interface; prior to failure a considerable fiber and cementitious matrix slip occurred; an effective bond length was about 250-300 mm in case of single layer; in case of two layers of PBO mesh the measured fiber strains at debonding was lower (roughly 85%) than that measured in case of single layer.

A bond-slip model based on experimental results of double shear test involving different anchorage lengths and fiber cross sections had been also proposed (D'Ambrisi et al. 2012a). The obtained bond-slip relationship was characterized by ascending branch (up to maximum shear stress around 0.6 MPa) and by a pronounced descending branch (up to slips larger than 1 mm). And the definition of the bond surface and of its dependency on the fibers arrangement and on the number of fiber layers was crucial in the determination of a bond-slip relationship.

However, those above results are still not clear or generic for applying every case of using PBO-FRCM systems. They need to be verified by more researches. Therefore, this study is conducted to investigate on the bond behavior between PBO-FRCM strengthening material and concrete with emphasis of effective bond length and bond stress-slip relationship.

2.3.3 The behavior of FRCM systems for strengthening RC structures

Tommaso et al. (2008) analyzed the behavior of RC beams strengthened with the FRCM system made of carbon fiber meshes and cementitious mortar. Results of these experimental investigated if the effectiveness of the FRCM system was both in terms of strength and ductility.

The FRCM system was recently improved by using PBO fibers. Mechanics properties of the PBO fiber are, in fact, fairly higher than that of the high strength type of carbon fibers, they have great impact tolerance, energy absorption capacity superior than the other kind of fibers, in addition PBO fibers demonstrate high creep and fire resistance (Wu et al. 2003).

Very few studies have investigated on the debonding phenomena in the strengthened beams with PBO-FRCM system. Recently, some experimental results carried out on PBO-FRCM strengthened RC beams (Tommaso et al. 2007, Ombres 2011a, 2011b) investigated if: (i) the flexural failure of FRCM strengthened beams was more ductile than the obtained for CFRP strengthened beams because of gradual

loss of composite action related to large slip at fiber/cementitious matrix interface; (ii) the debonding mechanism was governed by the concrete/matrix interface; (iii) the failure modes were depended on the amount of PBO fiber: for low values of PBO layers a typical flexural failure was observed while increasing the amount of PBO fibers layers the failure was due IC debonding.

Debonding phenomenon is an important characteristic to evaluate the effectiveness of any strengthening system and strongly depended on the load transfer mechanisms at the concrete/matrix interface. Because the transfer load mechanism of PBO-FRCM system was different from that of FRP system, so that the debonding process in PBO-FRCM strengthened RC beams was different than that observed in FRP strengthened RC beams. In fact, the debonding phenomena occurred in the concrete substrate in case of FPR systems and the debonding phenomena occurred within the cementitious matrix with in case of PBO-FRCM system.

In addition, predictions of debonding models of FRP strengthened RC beams were not accurate to apply for PBO-FRCM strengthened system when debonding failures occurred. Difference between predictions and experimental values, observed in terms both of ultimate capacity and debonding strains were, in fact, in the range 3-40% (Ombres 2011b). So that we continue investigating on the debonding behavior of beams strengthened with PBO-FRCM system under four-point flexural test in this research.

Chapter 3

Experimental program

3.1 General

Research program is conducted at the Structure Laboratory, Department of Civil Engineering, Faculty of Engineering, Chulalongkorn University. The usage of the PBO fabric meshes to make a FRCM system is still under investigation. This research project focuses on the debonding of externally bonded polypara phenylene benzobisoxazole (PBO) mesh for flexural strengthening of reinforced concrete beams.

There are three main objectives of this experimental program, including: 1) to determine the effective bond length of PBO mesh for PBO-FRCM system, 2) to establish the bond slip law between PBO mesh and concrete, and 3) to investigate the debonding behavior of PBO-FRCM strengthened RC beams under bending test.

3.2 Experimental program

The experimental program consisted of two phases. The first phase included the pullout test of 21 concrete prism specimens. The second phase included testing of 12 concrete beams strengthened beams in flexure using PBO-FRCM system.

The first phase included two parts: the first part included 12 specimens for determining the effective bond length of PBO in PBO-FRCM system and the second part included 9 specimens for establish the bond stress-slip between PBO and

concrete. And the second phase included 12 strengthened beams with PBO-FRCM under bending test to investigate the debonding behavior.

3.3 Phase I: Pullout test

Based on (Yao et al. 2005), we can classify the existing set-up of shear test into six types as shown in Figure 3.1: (a) double-shear pull test; (b) double-shear push test; (c) single shear pull test; (d) single shear push test; (e) beam test; and (f) modified beam test. These arrangements are based on the definition of the loading condition and on the symmetry of the system. The first four configurations of test method may also be called as pullout tests.

The configurations of (e) and (f) are indirect measured method. Asymmetrical configuration (c) and (d) are in general preferable to the symmetrical configuration of (a) and (b) because the symmetry of specimen can be lost when the debonding only starts on one side and prevents from following correctly the post peak behavior.

In addition, in intermediate crack induced debonding failure of strengthened beam with PBO-FRCM that almost occurred in beam under bending test of some previous research (Tommaso et al. 2007, Ombres 2011a, 2011b), the stress state in the critical region of the beam is also closely similar to that of the concrete prism in single-shear push test (d). Consequently, the single shear push test (d) was used in this study to investigate the bond behavior between PBO and concrete in FRCM strengthening system.
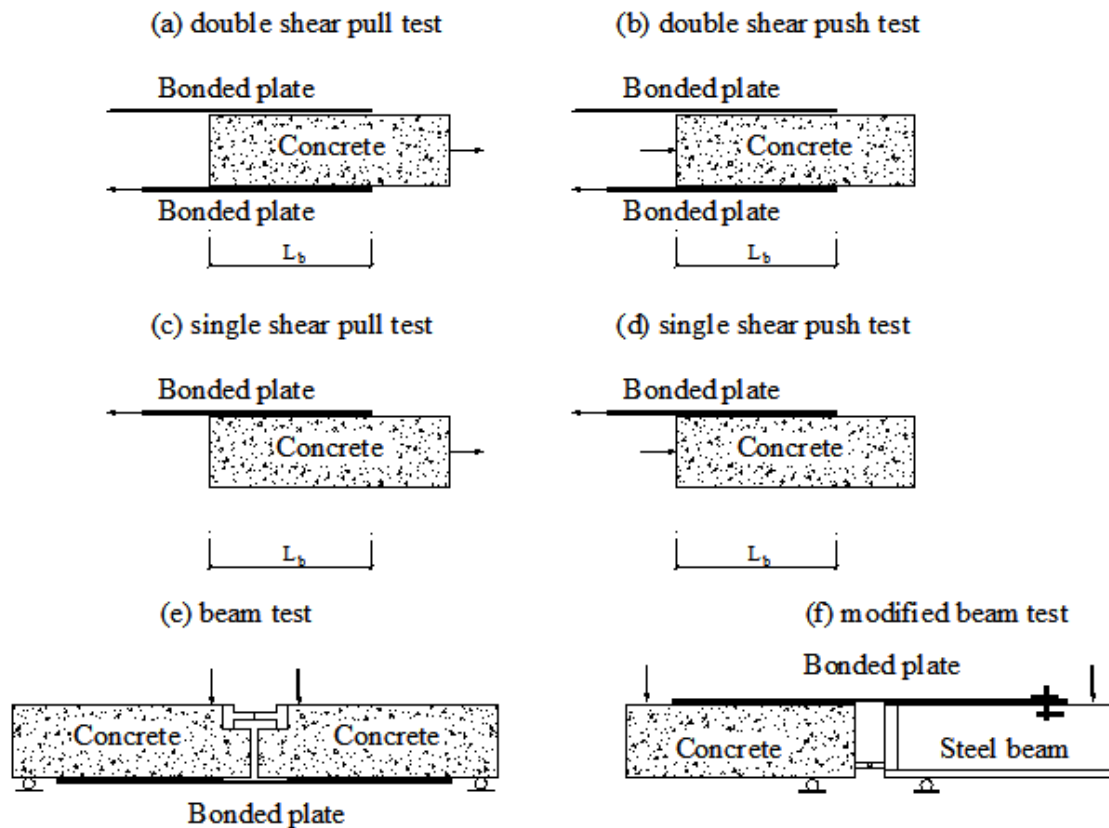
Figure 3.1 Classification of shear tests

3.3.1 Effective bond length

There are many researches on the bond behavior of FRP strengthening systems in literature (Hosseini and Mostofinejad 2014). The effective bond length can be defined as the length that extension of bond length of strengthening material beyond effective bond length does not increase capacity of bond strength. Consequently, effective bond length is one of important issues that need to be verified. Up to now, there are some researches on the bond behavior of PBO-FRCM system (Tommaso et al. 2008, D'Ambrisi et al. 2012a, 2012b, 2013) , however there are not any available

researches that have enough data to determine the effective bond length of PBO for PBO-FRCM strengthening system. Therefore, to investigate the effective bond length of PBO-FRCM, the pullout tests of PBO-FRCM in concrete specimens involving different bond lengths were conducted.

This part of experimental program represents the preliminary investigation for the bond behavior of the PBO-FRCM system.

3.3.1.1 Tested specimens

Material

The mechanical and geometrical characteristics of PBO mesh and cementitious matrix are report in Table 3.1 and Figure 3.2. The values in the table were provided by the manufacture of indicated in the previous study using the same PBO-FRCM system (D'Ambrisi et al. 2012b) The Poisson's ratio was assumed based on the available literature (Ohama 1995)

Table 3.1 Characteristics of the PBO mesh and cementitious matrix

	Unit	PBO mesh	Cementitious matrix
Tensile strength	(N/mm^2)	5800[a]	2.55[a]
Compressive strength	(N/mm^2)	-	16.1[a]
Young modulus	(GPa)	270[a]	6.144[a]
Failure strain	(%)	2.15[a]	-
Thickness	(mm)	0.0455[a]	1.44[b]
Poisson's ratio	-	-	0.18[c]

[a] referred to (D'Ambrisi et al. 2012b) and manufacture's value

[b] average value of experimental results

[c] referred to (Ohama 1995)

Figure 3.2 PBO and cementitous materials

Prism concrete

There were two types of concrete prism sized 100x100x500 mm with 41MPa of compressive concrete strength that were determined by compressive test of concrete cylinders as show in Figure 3.3
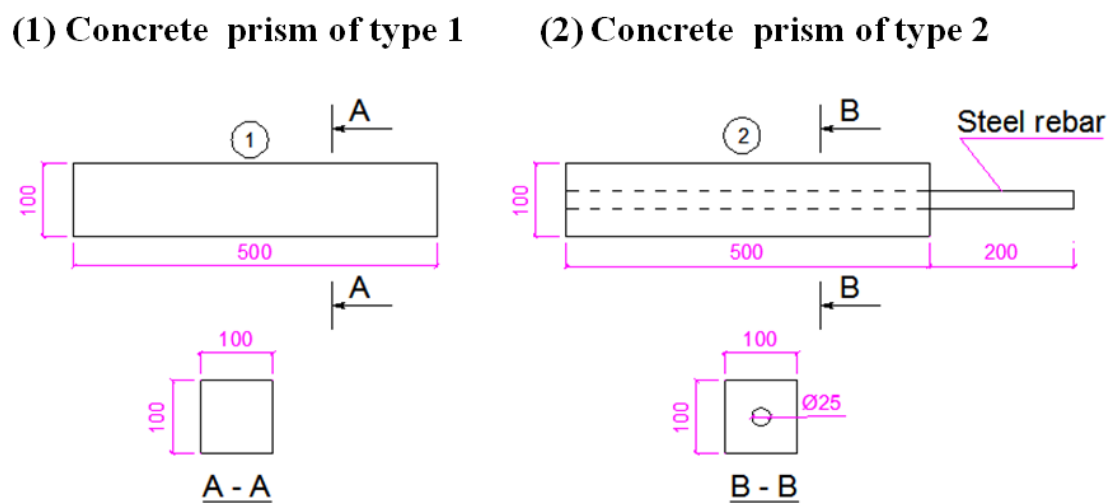
Figure 3.3 Details of concrete prisms

Fabrication of concrete prisms

All concrete prisms were cast by the steel moulds 100x100x500 mm, which were designed to insert steel rebar through in the middle section of each concrete prism of type 2 as shown in Figure 3.4. Before each casting, the moulds were cleaned and applied oil inside of surface to provide ease in specimen removal.

All concrete prism of effective bond length test were cast by ready mixed concrete and compacted by using a mechanical vibrator at the same time. Tested cylinders

were also cast at the same time of concrete prisms. Twenty hours after casting, the concrete prism and cylinders were removed to maintain in water. They were stored in the laboratory to complete 28 days. After 28 days, three concrete cylinders were tested in compression to determine the compressive strength of concrete.

(a) Steel moulds   **(b) Casting concrete prism**

Figure 3.4 Fabrication of concrete prism

Procedure for applying PBO-FRCM strengthening system

- Preparing the substrate

- Dust and loose parts of specimens was eliminated. Then the surface of specimens was rubbed gently by machine and cleaned by water to eliminate the thin layer of cement grout completely. The surface of specimens was flat after this operation.

- Preparing cementitious mortar

- First, about 90% of required amount of water was poured into mixer, then the mixer was started and cementitous power, Ruredilxmesh 750, was added uninterruptedly to prevent lumps from forming. After mixing for 2-3 minutes, the rest of the water up to the quantity specified in the technical information sheet was added and mixed for 1-2 minutes more. After 2-3 minutes, the mixture was mixed again and applied.

- Applying PBO-FRCM strengthening system:

- The substrate was dampened and saturated with water. Cementitous mortar was applied with a smooth metal trowel in a layer about 3-4 mm thickness. After a couple of minutes, PBO mesh was buried and gently pressed in it by rolled tool. After that, a second layer of cementitious was applied to cover the PBO mesh completely. This procedure was repeated until attaching enough PBO layers that were designed.

Fabrication of tested specimens

The tested specimens were made of two types of concrete prism combined by bonded PBO-FRCM strength system on one surface of two concrete prisms after curing for 28 days as show in Figure 3.5. U-GFRP wraps were used to anchor PBO mesh to concrete prism of type 2. There are three specimens for each group with

different bond length L of 250, 300, 350 and 400 mm. The compressive concrete

strength of all tested specimens was 41 MPa
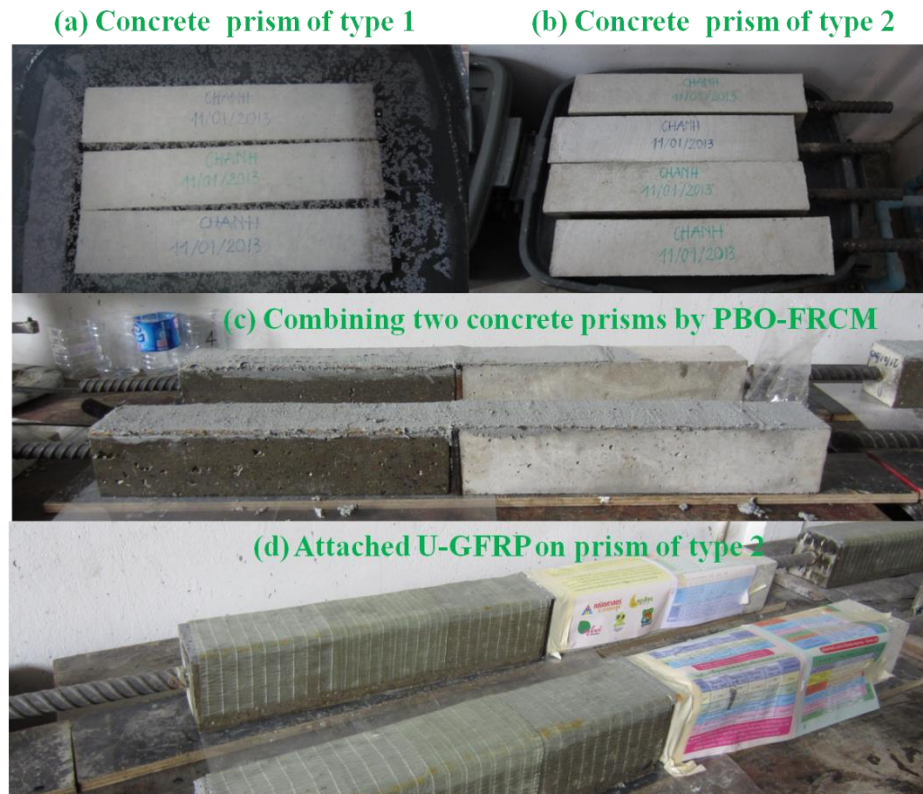
Figure 3.5 Fabrication of tested specimens

3.3.1.2 Test setup

The tested specimen was positioned on a rigid steel frame in order to prevent from

horizontal and vertical displacements as shown in Figure 3.6. The load is applied

through steel rebar of concrete prism of type 2 and rigid frame as shown in Figure

3.7. During the pull out test procedure, the displacement controlled loading system

was applied by Instron machine and the speed rate was 0.1 mm/min. The maximum

load and corresponding bond length were intended to be obtained. And loads were

recorded by data logger during the test.

Figure 3.6 Tested specimen in rigid frame
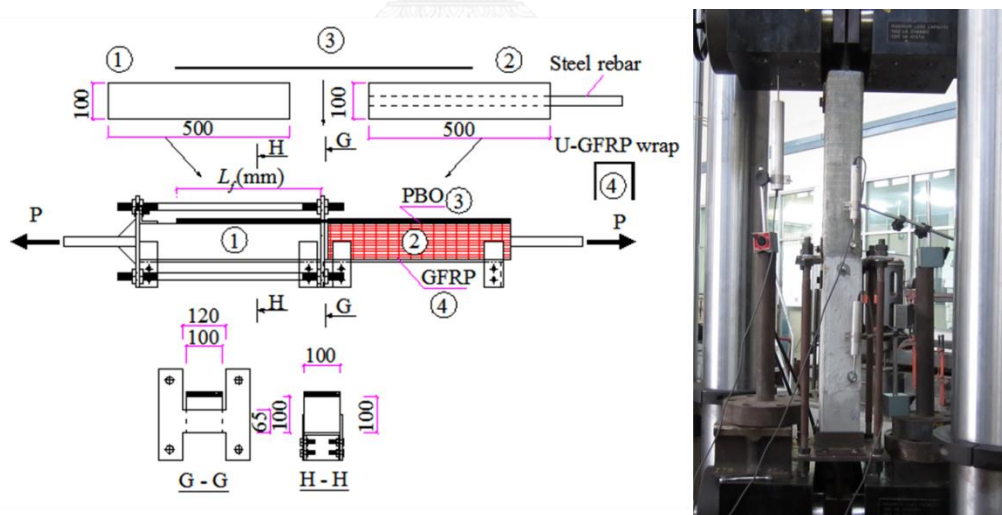
Figure 3. 7 Test setup for effective bond length

Details of specimens in effective bond length are shown in Table 3.2, where the

specimens names are m-n, in which m indicates the bond length of PBO mesh, n

identifies a single specimen among the same group of bond length ($n = \overline{1:3}$). f_c' is the compressive strength of concrete which were determined under compressive test of concrete cylinders. L_f, b_f and n_f are the bond length, the width and number layers of PBO mesh, respectively.

Table 3.2 Description of specimens for effective bond length test

Specimens (m-n)	f_c' (MPa)	L_f (mm)	b_f (mm)	n_f	Total of specimens
250-n	41	250	100	1	3
300-n	41	300	100	1	3
350-n	41	350	100	1	3
400-n	41	400	100	1	3

3.3.2 Bond stress-slip test

Bond strength between strengthening material and concrete substrate is a key factor to evaluate effectiveness of any strengthening system. Consequently, investigation on the bond behavior between PBO and concrete is very necessary to understand about the PBO-FRCM strengthening system completely. In addition, until now, the bond strength between PBO and concrete are under investigation and it need to be verified by more researches.

The procedure of test was similar with effective bond length test, but the bond lengths of all specimens are the same. The compressive strengths of concrete substrate (31, 41 and 39 MPa) were determined under compressive test of concrete cylinders.

3.3.2.1 Test specimens

The materials, size of concrete prism and process of fabrication of tested specimens for bond stress-slip are the similar to those for effective bond length test as shown in Figure 3.8. However, in process of fabrication, before attaching PBO mesh to combine two concrete prisms, we had one more process in order to can apply strain gauges on the PBO mesh. To obtain the accurate geometrical information about the cementitious layer, the tested specimens were processed after the pullout test. They were cut by machine and then the thickness of each cementitious layer was measured under a microscope. In addition, three types of compressive concrete strength were considered in this section.

Procedure for applying PBO-FRCM strengthening system

The procedure of applying PBO-FRCM for specimens of bond stress-slip test were conducted step by step which was similar to that of effective bond length test. However, in this test, there was one more procedure of applying strain gauges on PBO mesh due to measure the strain of PBO mesh.

Procedure of applying strain gauges on PBO mesh

- PBO mesh was cut in the size of specimen, then determining and marking the area on which was applied the strain gauges (with pen)

- The marked area of PBO mesh was soaked by appropriate glue (CC-33A) for strain gauges. After the glue had dried, a masking tape was applied to cover area of the glue completely.

- The first layer of cementitious mortar was applied on the specimen. Then the PBO mesh was buried and gently pressed in it. After that, while the second layer of cementitious mortar was been applying to cover the PBO mesh, the location of the tape was being pointed.

- After the second mortar had applied for some minutes, the masking tape was removed by tweezers.

- Strain gauges were applied on the marked area of PBO mesh when the surface of cementitious mortar had hardened. After that, they were covered by cementitous mortar.

(a) Strain gauges and glue (Kyowa)   **(b) Attaching strain gauge on PBO**

Figure 3. 8 Tested specimen for bond stress-slip test

All tested specimen had the same characteristics with 400 mm of bond length of PBO mesh and seven strain gauges that were attached on the surface of PBO mesh with constant interval (~55mm) for measuring strain of PBO as shown in Figure 3.8.

3.3.2.2 Test setup

The configuration of bond stress-slip test was the same with effective bond length test. The specimens were tested under pullout test by using rigid steel frame as shown in Figure 3.9. The applied loads were controlled by Instron machine. The speed of displacement controlled loading was 0.1 mm/min. The applied load and strain of PBO mesh was recorded by data logger.
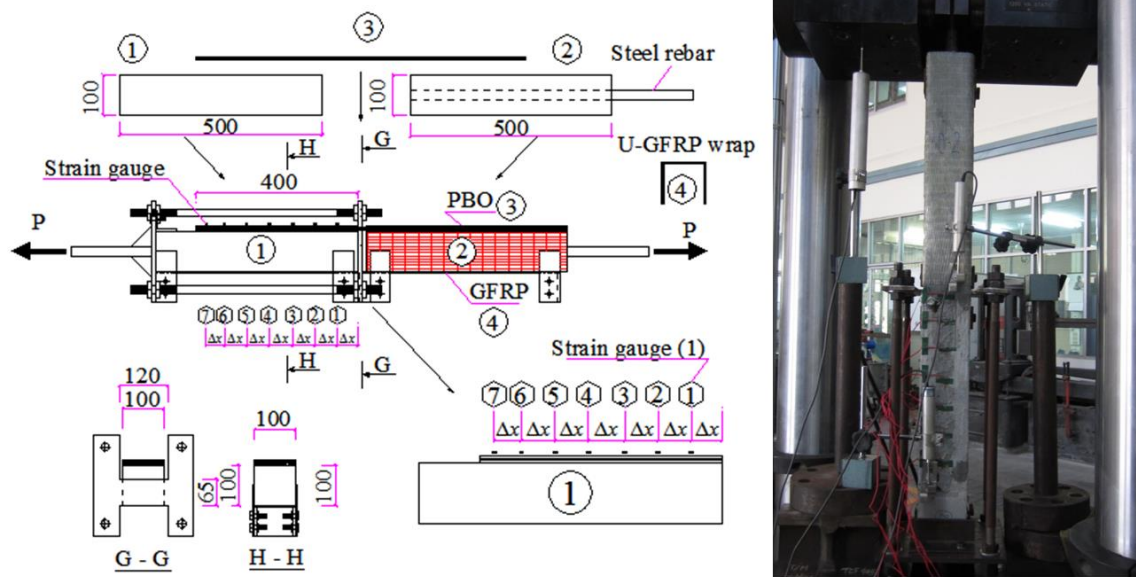
Figure 3. 9 Setup of bond stress-slip test

Table 3. 3 Description of specimens for bond stress-slip test

Specimens	f_c' (MPa)	L_f (mm)	b_f (mm)	n_f	Number of specimens
S1-1	31	400	100	1	1
S1-2	31	400	100	1	1
S1-3	31	400	100	1	1
S2-1	41	400	100	1	1
S2-2	41	400	100	1	1
S2-3	41	400	100	1	1
S3-1	39	400	100	1	1
S3-2	39	400	100	1	1
S3-3	39	400	100	1	1

Table 3.3 shows the details of specimens for bond stress-slip test, where the names

of specimens are of type Sk-n, in which k is the notation of compressive concrete

strength group and $k = \overline{1:3}$ corresponding with 31, 41, 39 MPa of compressive

concrete strength, n identifies a single specimen among the specimens with the same characteristics.

3.4 Phase II: Bending test

Some available data of previous researches (Tommaso et al. 2007, Tommaso et al. 2008, Ombres 2009, 2011a), debonding failures can take place at the end of the strengthening plates in presence of high stress at the interface between the strengthening system and the concrete (end debonding) or away from the ends of the bonded strengthening plates when they are induced by flexural or flexural-shear cracks (IC debonding). The results of those researches investigated if increasing the percentage of PBO fibers and the failure of beams was potentially due to IC debonding. Therefore, this research is focus to study the mechanism of the intermediate crack induced debonding (IC debonding) on the flexural beams strengthened PBO-FRCM.

The experimental program was conducted to investigate the IC debonding behavior of RC beams strengthened with PBO-FRCM system. The effectiveness of the number of PBO layers and compressive strength of concrete were considered in this study. The results of tests evidenced that the IC debonding was the main failure mode of RC beams strengthened with PBO-FRCM system under four-point bending test.

3.4.1 Tested specimens

A total of 12 reinforced concrete beams were strengthened by PBO-FRCM system involving different parameters such as compressive strength of concrete and PBO layers. The beams were tested to failure. The beam has size of 100x180x1800 mm. There are three groups of beam corresponding with compressive strength of concrete, series B1, B2, and B3. In each group, the beams were strengthened by various PBO layers. All of beams were designed to be under flexure and having flexural failure. U-GFRP and inverted U-GFRP were combined to strengthen shear capacity of beams to prevent from shear failure. The first series, B1 has 31 MPa of compressive strength of concrete, while B2 has 41 MPa of compressive strength of concrete, and the third series B3 has 39 MPa of compressive strength of concrete. Two 12 mm diameter steel rebars and two 10 mm diameter steel rebars were used as compression and tension reinforcement for all beams, respectively. And 6 mm diameter steel stirrups were used in all beams with spacing 100 mm over all the length of the beam to prevent shear failure. Figure 3.10 shows the dimensions and the reinforcement of beams

The compressive strengths of concrete were determined by compressive tests of concrete cylinders that were cast at the same time with the tested beams after 28 days. The average strengths of concrete are reported in Table 3.4. The yielding strength of tensile rebars and compressive rebars are also reported in Table 3.4

Table 3. 4 Material properties

Beam series	f'_c (MPa)	f_{ct} (MPa)	E_c (GPa)	Rebar diameter	ε_y	E_y (GPa)	f_y (MPa)
B1	31	3.12	26.2	12	0.0028	200	560
				10	0.003	150	450
B2	41	3.59	30	12	0.0028	200	560
				10	0.003	150	450
B3	40	3.50	29.4	12	0.0028	200	560
				10	0.003	150	450
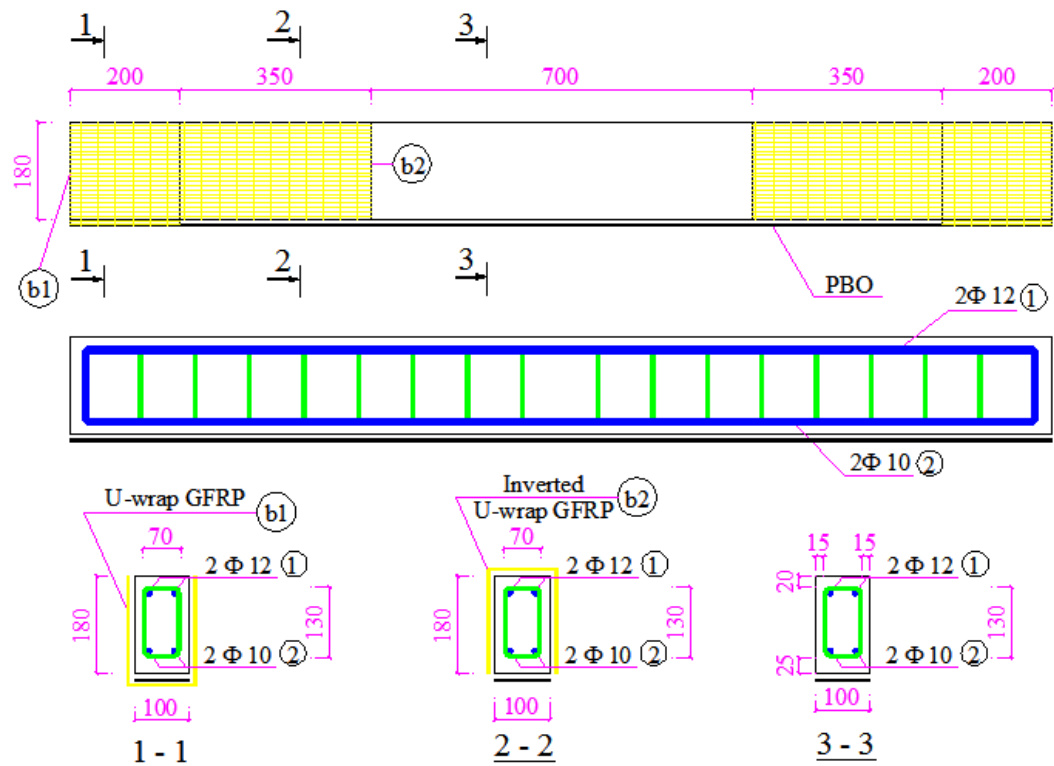
Figure 3. 10 Dimensions and reinforcement details of tested beam

Fabrication of tested beams

The beams were cast in steel moulds which were designed so that four beams to be cast at each time. The steel moulds have the same size 100x180x1800 mm of the specimens. The moulds were re-used 3 times for casting the 12 beams. The moulds were cleaned and lubricated to provide ease in the beam removal before each casting. The reinforcement cages were assembled, tied and placed in the moulds as shown in Figure 3.11

(a) Reinforcement cages and steel moulds　　**(b) Casting beams**

(c) Curing of beams

Figure 3. 11 Fabrication and curing of beams

There were four series of beams corresponding with compressive strengths of concrete. All beams of each group were casted by using ready-mix concrete at the same time. Tested cylinders were cast at the same time of the beams. After 24 hours, the beams were removed out of mould and curved by covering them with wet burlap to keep them wet while the concrete cylinders also were removed to curing by water. The burlap had been kept wet all the time during the curing period of 28 days. After 28 days, three cylinders were tested in compressive test from each patch to determine the compressive strength of concrete.

Procedure of strengthening PBO-FRCM

After 28 days, all beams were turned upside down to be prepared for the surface of beams before applying PBO-FRCM system. The locations of PBO-FRCM were marked on the tension side of beams. Then the procedure of applying PBO-FRCM and that of applying strain gauges on PBO were the similar with pullout test. In case of strengthened beam with more one layer, the PBO mesh that were designed to applying strain gauges were attached as the last to be applied on beam.
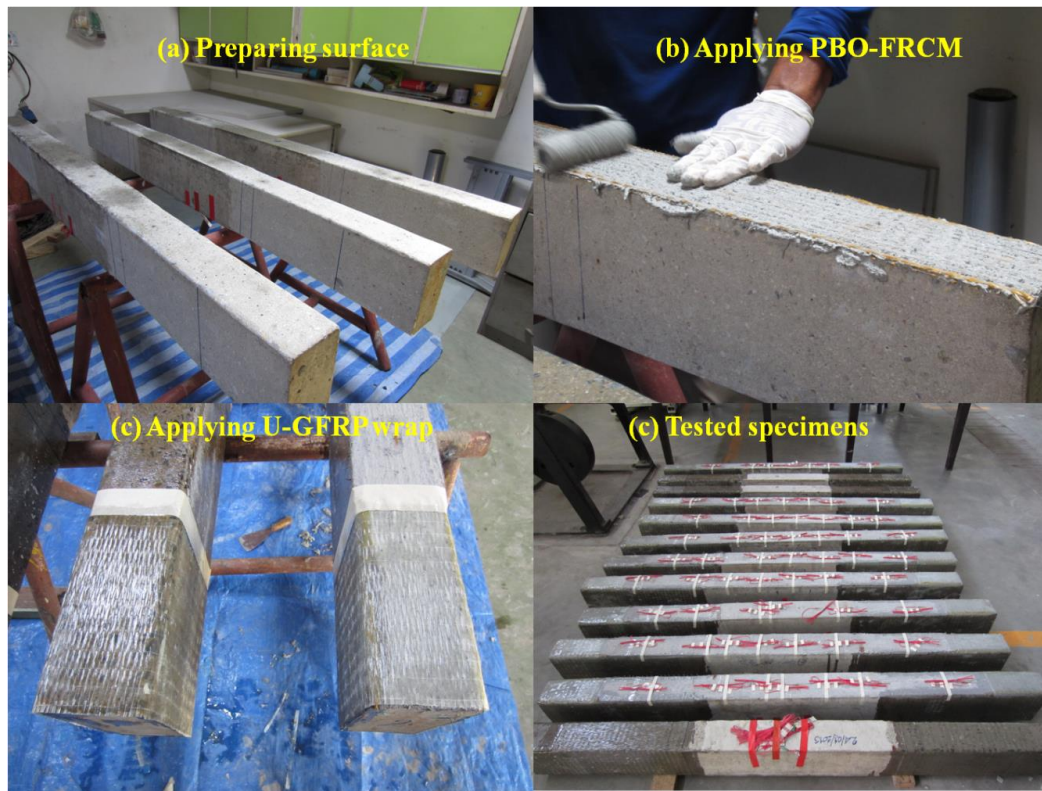
Figure 3. 12 Fabrication of tested beams

Table 3. 5 Description of tested beams

Beam	$bxhxl$	f'_c (MPa)	A'_s (mm^2)	A_s(mm^2)	n_f	b_f (mm)
B1-1	100x180x1800	31	226	157	1	100
B1-2	100x180x1800	31	226	157	2	100
B1-3	100x180x1800	31	226	157	3	100
B2-1	100x180x1800	41	226	157	1	100
B2-2	100x180x1800	41	226	157	2	100
B2-3	100x180x1800	41	226	157	3	100
B3-1	100x180x1800	39	226	157	1	100
B3-2	100x180x1800	39	226	157	2	100
B3-3	100x180x1800	39	226	157	3	100

The tested beams were designed to prevent the premature of shear failure. They are named following labels: the first letter "B" and the first number (1, 2 or 3) indicate the series of tested beams (B1, B2 or B3); the second number (1, 2 or 3) indicates the PBO layers applied on the concrete surface. For example B1-1 shows that the beam belongs to series B1 and there is one attached PBO layer on this beam. Details of specimens are reports in Table 3.5

Instrumentation

The instrumentation that was used to monitor the behavior of beams during testing consisted of a combination of electrical strain gauges and linear variable differential transducers (LVDT) with different stroke lengths as shown in Figure 3.13

Strain gauges were used to capture the strains for the concrete, steel and PBO mesh. Before casting concrete of beam, four strain gauges had been installed on tensile steel rebars and compressive steel rebars at the mid-span of beams. Two strain gauges were installed on the top and bottom of concrete surface at the mid-span of beam. Other seven strain gauges were installed along the surface of PBO. The distribution of the strain gauges is shown in Figure 3.13

Figure 3. 13 Distribution strain gauges on the tested beams

Strains monitoring

Different electrical strain gauges were used to capture the strains for the concrete, steel and PBO mesh. All the electrical strain gauges used were produced by Kyowa Electronic Instruments Co., LTD., Tokyo Japan as shown in Figure 3. 14

Figure 3. 14 Strain gauges

Before casting concrete of beam, two strain gauges with a gage length of 2 mm had been installed on the mid-span of the tensile steel of beam, and two strain gauges with a gage length of 2 mm had been installed on the mid-span of the compressive steel of beam. A limited area that fitted with area of strain gauge on the steel rebars was smoothened. The strain gauges were glued on the smooth area of steel rebars by using CC-33A. After applied glue had dried, the locations of strain gauges were covered by tape to protect strain gauges from the water and damage during casting.

Other two strain gauges with gage length 70 mm were installed on the mid-span of the top and bottom of the concrete to measure the strain in concrete.

Seven strain gauges with gage length of 2 mm were installed along the surface of PBO mesh. The procedure of applying strain gauges on PBO mesh had to do them same specimens of pullout test.

Deflection monitoring

The deflection at mid span was monitored by using LVDT with stroke length of 100 mm. Other two LVDT with stroke length of 50 mm were placed at two the support of beam as shown in Figure 3. 15

Figure 3. 15 Deflection monitoring

Readings from load cell of Instron machine, strain gauges and LVDTs were recorded

during the test by using data logger Universal Recorder EDX-100A (manufactured by

Kyowa), which was connected to a computer as shown in Figure 3. 16.
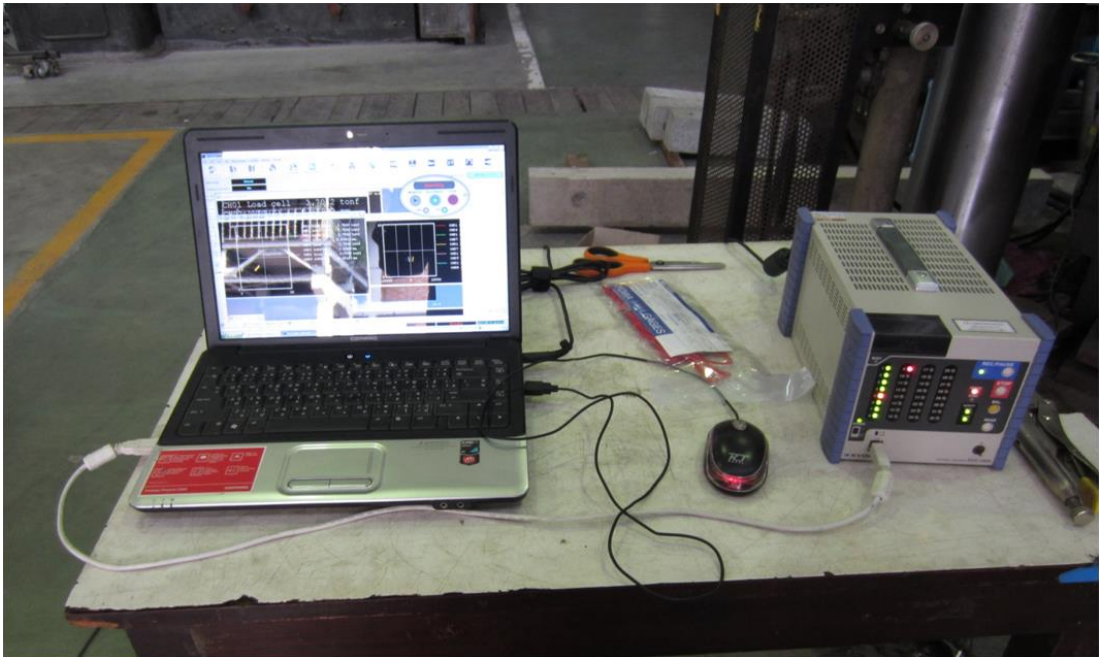
Figure 3. 16 Universal recorder EDX-100A

3.4.2 Test setup

The beams were tested under four-point bending over a simply supported clear span of 1500 mm. Displacement controlled load were used by Instron machine and the speech rate of load were 0.2 mm/min. The load was applied on the beam through a steel I-beam with the full width of beam as shown in Figure 3. 17. The applied load, strain gauges and LVDTs were connected to data logger by the connector tools and were recorded during the test.

Figure 3. 17 Test setup of bending test
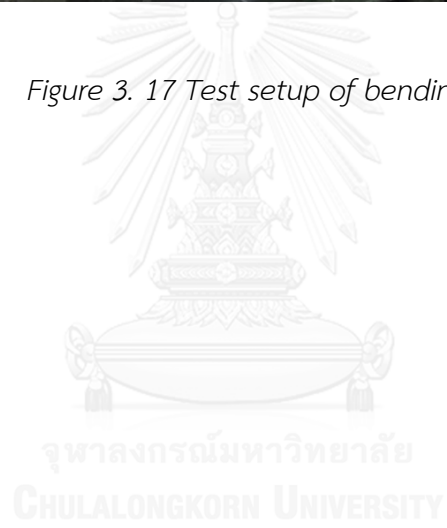
Chapter 4

Bond behavior: Analysis and discussion of test results

4.1 General

The effectiveness of PBO-FRCM strengthening system depends strongly on the bond stress and transfer load from the concrete to PBO mesh through cementitious bonding agent. And there is an existing effective bond length that extension of bond length beyond the effective bond length do not increase maximum transfer load of PBO-FRCM system. Therefore, the bond stress-slip relationship between PBO-FRCM and concrete is very important characteristics to understand about the PBO-FRCM system thoroughly before using and applying this strengthening system in practice widely. Therefore, in the first of this study, the bond behavior between PBO and concrete were carried out by pullout test of PBO-FRCM strengthening system.

The pullout test included two stages. The first stage included 12 tested specimens to determine the effective bond length of PBO for PBO-FRCM strengthening system; while the second stage phase included 9 tested specimens to investigate bond stress slip relationship between PBO and concrete.

4.2 Effective bond length

In this stage, 12 specimens were repaired and tested under pullout test. The important parameter in here is the bond length of PBO, maximum load and failure mode. The results of these specimens were analysed and discussed in this section.

4.2.1 Experimental results

Debonding phenomena occurred in all tested specimens at the PBO mesh and cementitious matrix interface after considerable fiber slip when the PBO mesh configuration became visible through FRCM layer as shown in Figure 4. 1.
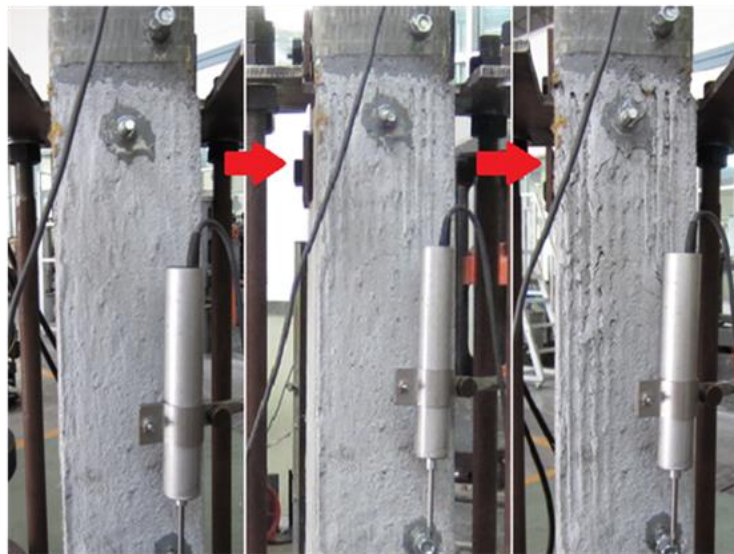
Figure 4. 1 Debonding phenomena in pullout test

Figure 4.1 shows that cracks had formed at loaded end of specimen first, and then they propagated to the free end of tested specimens until debonding occurred in specimen. And the debonding phenomena occurred within the cementitious layer. In fact, there was still a thin layer of matrix remained perfectly attached to the concrete surface as shown in Figure 4. 2. This phenomena is similar to results of previous research (D'Ambrisi et al. 2012b).

Figure 4. 2 Thin layer of cementitious after debonding

Table 4. 1 Results of effective bond length test

Specimen (m-n)	f'_c (MPa)	b_f (mm)	L_f (mm)	P_{max} (kN)	$P_{av,max}$ (kN)	Failure mode
250-1	41	100	250	10.92		DB
250-2	41	100	250	11.36	10.95	DB
250-3	41	100	250	10.58		DB
300-1	41	100	300	11.05		DB
300-2	41	100	300	10.20	10.94	DB
300-3	41	100	300	11.58		DB
350-1	41	100	350	10.30		DB
350-2	41	100	350	9.95	10.46	DB
350-3	41	100	350	11.14		DB
400-1	41	100	400	9.95		DB
400-2	41	100	400	10.51	10.78	DB
400-3	41	100	400	11.86		DB

DB: debonding

which

- P_{max} is the maximum load

- P_{av} is the average of maximum load

- f'_c is compressive strength of concrete

- b_f is the width of PBO mesh

- L_f is the bond length of PBO

The main tested results of effective bond length test are summarized in Table 4.1, where the "m" in the specimen name means the bond length of PBO and "n" identifies a specimen among the series of specimens with the same bond length.

4.2.2 Effective bond length

Experimental results show that the maximum loads are regarded as constant value for the bond lengths L from 250 mm to 400 mm and the average of P_{max} equals to 10.78 as shown in Figure 4.3. In fact, there is a variation among the maximum loads probably due to non-uniform stress distribution among fibers in roving, or the different thickness of cementitious layer, or the different constitution of concrete substrate surface in various specimens.
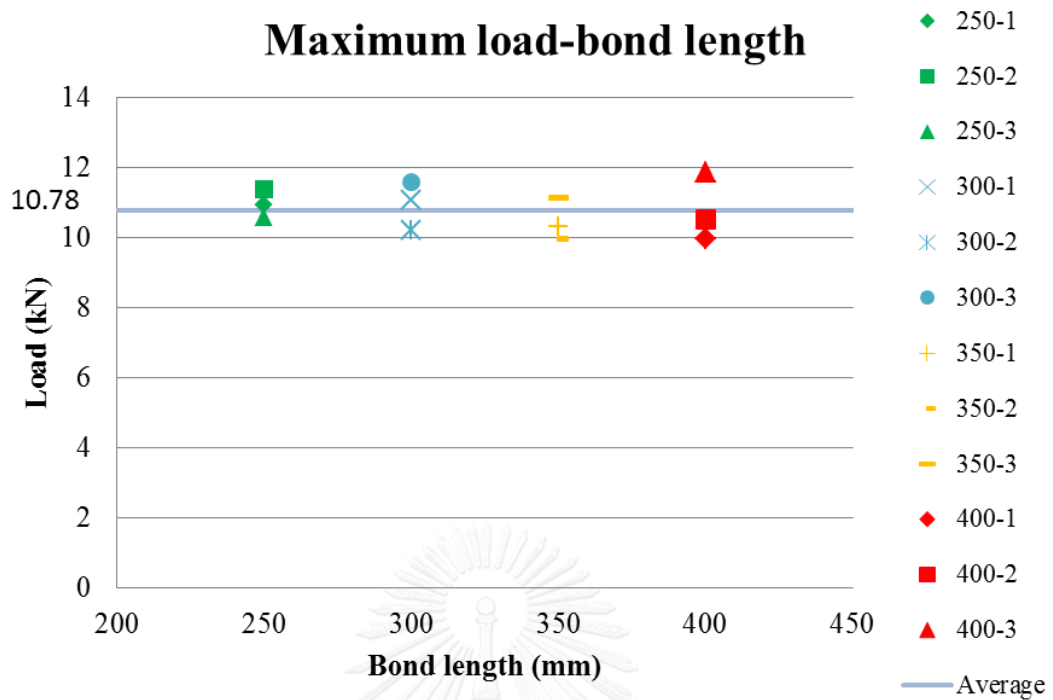
Figure 4. 3 Relationship between maximum load and corresponding bond length of

PBO

Figure 4.4, in which the experimental results of previous research (D'Ambrisi et al. 2012b) as well as those in this study are shown, shows that the relationship between P_{max} and corresponding bond length of PBO mesh is rather linear until the bond length reaches 250 mm, and P_{max} can be regarded as constant value for the bond length over 250 mm. So that the effective bond length of PBO for the PBO-FRCM system is around 250 mm.

Maximum load-bond length
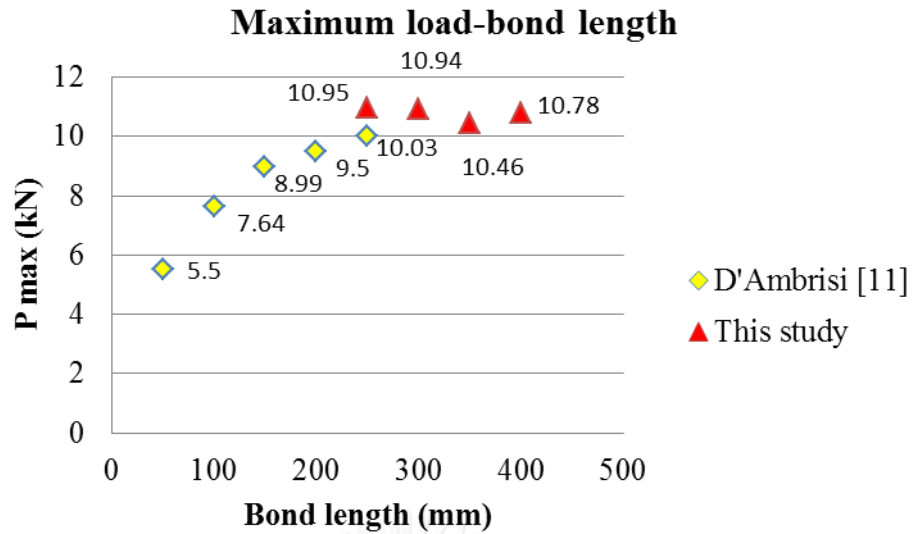
Figure 4. 4 Relationship between P_{max} and corresponding bond length of PBO in this study and previous research (D'Ambrisi et al. 2012b)

Comparison between effective bond length of PBO-FRCM system and that of conventional CFRP system

There are many researches on the bond behavior of FRP strengthening system in literature (Hosseini and Mostofinejad 2014). They conclude that there is an existing effective bond length of FRP for each FRP system; it means that extension of bond length of FRP material beyond effective bond length does not increase capacity of bond strength. Therefore, effective bond length is one of important issues that need to be verified. Many models have been proposed to predict effective bond length of FRP system. However, only a few of them, which were derived from experimental data, has been accepted by design guidelines such as ACI-440.2R (2008) and HB-305

(2008). Model of Chen and Teng (2001) presented in ACI 440.2R (ACI-440.2R 2008),

model of Seracino et al. (2007) presented in HB 305 (HB-305 2008), and model of Dai

et al. (2005b) based on a larger number of experiments are showed in Table 3.

Table 4. 2 Models of effective bond length for FRP system and calculated results

Model	Effective bond length L_e (mm)	PBO-FRCM L_e (mm)	Remarks
Chen and Teng (2001)	$\sqrt{\dfrac{E_f t_f}{\sqrt{f_c'}}}$	44	
Seracino et al. (2007)	$\dfrac{\pi}{2\sqrt{\dfrac{\tau_f L_{per}}{\delta_f E_f A_f}}}$	22	$\tau_f = \left(0.802 + 0.078\dfrac{d_f}{b_f}\right)(f_c')^{0.6}$ $\delta_f = \dfrac{0.73}{\tau_f}\left(\dfrac{d_f}{b_f}\right)^{0.5}(f_c')^{0.67}$ $d_f = 1; L_{per} = 2d_f + b_f$
Dai et al. (2005b)	$0.74\sqrt{\dfrac{E_f t_f}{f_c'^{0.236}}}$	53	

For the PBO-FRCM system the effective bond lengths calculated by model of Chen

and Teng (2001), the model of Seracino et al. (2007) and the model of Dai et al.

(2005b) are 44, 22 mm and 53 mm respectively, which were much smaller than

experimental results (around 250 mm as shown in Fig. 6). It means that transfer stress

area of PBO-FRCM system was larger than that of FRP system. So that if debonding

occurred in two systems at the same level of load, the maximum bond stress of FRP

system would be higher than that of PBO-FRCM system. The reason of the

differences between PBO-FRCM system and FRP system could be due to the

difference between cementitious matrix and epoxy matrix. When load transferred between PBO and concrete, a lot of micro cracks in cementitious matrix would occur to extend the stress area in PBO material gradually. And the process of transfer load would continue until debonding occurred.

4.3 Bond stress-slip relationship between PBO-FRCM and concrete

In this stage, 9 specimens were repaired and tested under pullout test. The important parameter in here is effectiveness of compressive strength of concrete, and the bond behavior between PBO-FRCM and concrete.

4.3.1 Experimental results

The strain distribution of PBO meshes along the interfaces corresponding to every step load can be obtained by many strain gauges. The average local bond stress can be obtained using the following expression:

$$\bar{\tau}_i = \frac{E_f t_f (\varepsilon_i - \varepsilon_{i+1})}{x_{i+1} - x_i} \; with \; i = 1 \cdots 7 \tag{1}$$

where $\bar{\tau}_i$ is the average interfacial bond stress in the section i; ε_i and ε_{i+1} are the strain values of ith and $(i+1)^{th}$ strain gauges on PBO mesh respectively. E_f and t_f are the elastic modulus and thickness of PBO mesh respectively.

We assume that the strain of concrete can be neglected and the free end slip can be regarded approximately as zero in the case of using a long bond length. Therefore, the local slip can be expressed as:

$$s_i = \sum_{k=i}^{7} \frac{\varepsilon_k + \varepsilon_{k+1}}{2}(x_{k+1} - x_k) \ with \ i = 1 \cdots 7 \qquad (2)$$

where s_i is the local slip between PBO meshes and concrete at the section i; ε_8 is strain of PBO at the free end of bond area.

Average slip $\bar{s}_i$ to be coupled with corresponding average bond stress $\bar{\tau}_i$ can be finally obtained as follows:

$$\bar{s}_i = \frac{s_i + s_{i+1}}{2} \ with \ i = 1 \cdots 7 \qquad (3)$$

Similar to shear test for effective bond length, debonding failure occurred in all tested specimens (Fig. 7). The experimental results are summarized in Table 4, where f'_c is compressive strength of concrete, P_{max} is the force at debonding, $\bar{\tau}_{max}$ is maximum bond stress calculated by formula (1), $P_{av,max}$ is average of maximum load and $\bar{\tau}_{av,max}$ is average of maximum bond stress.

If the bond length of PBO L is longer than effective bond length L_{eff} , the interfacial fracture energy G_f at debonding can be obtained by the following equation

$$G_f = \int_0^\infty \tau(s)ds = \frac{P^2{}_{max}}{2b_f E_f A_f} \qquad (4)$$

b_f, A_f are the width and area section of PBO mesh, respectively, the latter of which can be calculated by the following equation

$$A_f = b_f t_f \qquad\qquad (5)$$

Table 4. 3 Experimental results

	f'_c (MPa)	b_f (mm)	L_f (mm)	P_{max} (kN)	$\bar{\tau}_{max}$ (MPa)	G_f (N/mm)	$\bar{P}_{av,max}$ (kN)	$\bar{\tau}_{av,max}$ (MPa)	$\bar{G}_f$ (N/mm)	Failure mode
S1-1		100	400	9.20	1.43	0.345				DB
S1-2	31	100	400	8.98	1.10	0.328	9.81	1.42	0.396	DB
S1-3		100	400	11.23	1.73	0.514				DB
S2-1		100	400	10.26	1.60	0.429				DB
S2-2	41	100	400	11.27	2.05	0.517	10.70	1.64	0.467	DB
S2-3		100	400	10.58	1.28	0.455				DB
S3-1		100	400	9.64	1.45	0.378				DB
S3-2	39	100	400	10.26	1.13	0.429	10.13	1.31	0.418	DB
S3-3		100	400	10.48	1.35	0.447				DB
Average							10.21	1.46	0.424	DB

DB: debonding
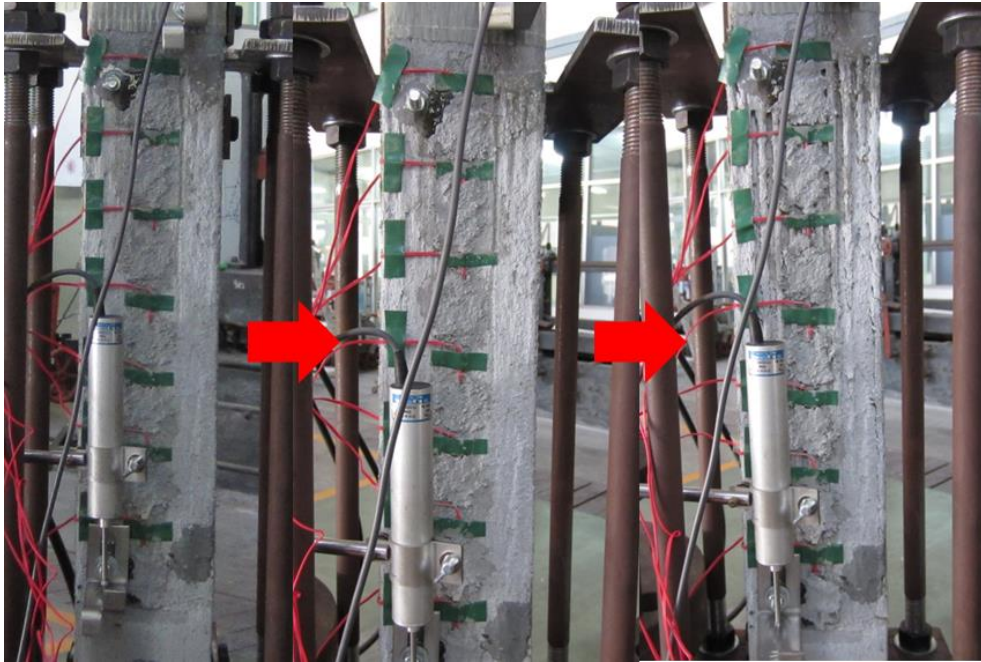
Figure 4. 5 Deboding failure of tested specimens

Based on the experimental results as shown in Table 4.3 and Fig 4.6, the maximum

load P_{max} slightly increase with substrate concrete strength although the debonding

occurred at interface concrete and FRCM rather than substrate concrete and FRCM. It

implies that the strength/stiffness of substrate concrete could affect the debonding

criteria at PBO mesh and FRCM.
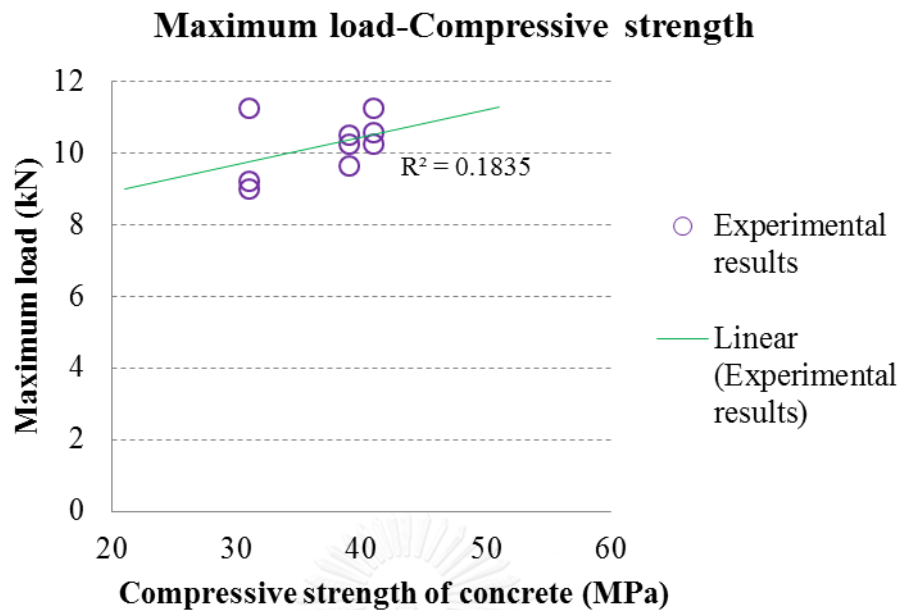
Figure 4. 6 Relationship between compressive strength of concrete and maximum

load in shear test

Figure 4.7a shows the relationship between the loads and corresponding PBO strain

at each location on the surface of PBO in specimens S1-1. Similar phenomena

occurred in almost all the tested specimens. It can be observed that the PBO strain

at location 1 (at a distance of 50 mm from the loaded end of the specimen)

increased first when load is applied. The load-strain relationship at location 1 was

regarded as linear until the applied load reached close to the maximum load. The

PBO strain at location 2 (at the distance of 105 mm from the load end) also started

when the applied load reached close to the maximum load. After that, the applied

load was constant at the value of maximum load and the PBO strain at location 1

also were regarded as constant while the PBO strain at location 2 continued to

increase. When the PBO strain at location 2 reached the PBO strain at location 1, debonding occurred.
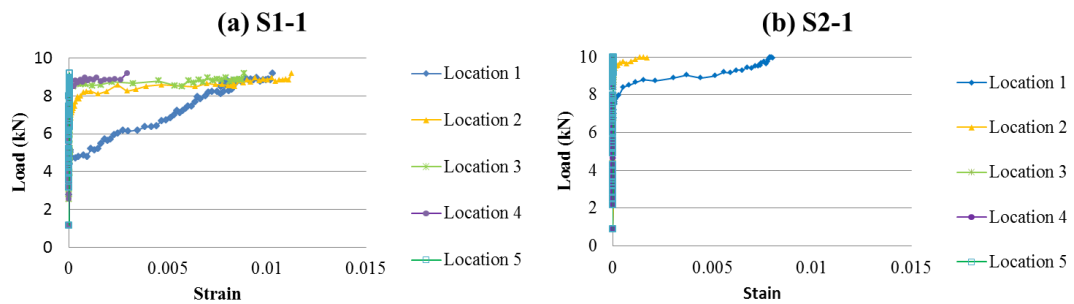
Figure 4. 7 Relationship between load and corresponding strain of each strain gauge on surface of PBO mesh until debonding: (a) in specimen S1-1 and (b) in specimen S2-1

There were two cases (S2-1 and S3-1) where the development of the local PBO strain occurred in a different manner as shown in Figure 4.7b. At the early stage of loading, the progress of the local PBO strain development in these specimens was the same as in the other specimens. The load-strain relationship of location 1 (at the distance of 50 mm from the loaded end of the specimen) was regarded as bi-linear until the applied load reached close to the maximum load. The PBO strain at location 2 (at the distance of 105 mm from the load end) also started to be developed when the applied load reached close to the maximum load. However, the strain development curve at location 1 of specimen S2-1 was similar to that at location 2 of specimen S1-1. This implied that the load transfer from loaded end to

free end of specimen S1-1 was more progressive than that of specimen S2-1. The differences here may be due to the different local bond property between PBO and the concrete substrate along the surface of the bond length in those specimens, which was caused when the specimens were made.
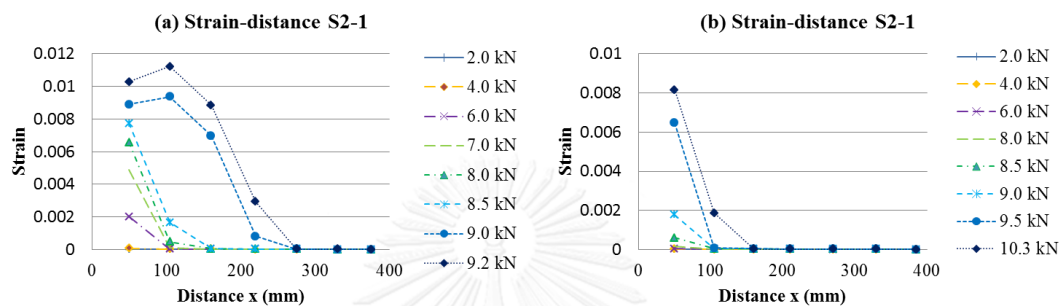
Figure 4. 8 Strain distribution of PBO at different load steps: (a) in specimen S1-1 and

(b) specimen S2-1

Figure 4.8a Figure 10a shows the strain distribution of PBO during the test on specimen S1-1. In this figure, the strain of PBO near the loaded end started to increase first when the load was applied on the specimens. After that, the strain of PBO transferred from the loaded end to the free end gradually when the applied load continued to increase. When the applied load reached close to the maximum load, the strain of PBO near the loaded end reaches the maximum strain and keeps the maximum strain while the applied maximum load was maintained. On the other hand the strain of PBO behind the loaded end area continued to increase until debonding occurred in the specimen. This progress implied the area of load transfer

moved from the loaded end to the free end. This behavior was similar among most of the tested specimens. However, as mentioned previously, the behavior of specimen S2-1 and S3-1 were of a different manner due to local debonding. The strain distributions of those specimens are shown in Fig. 10b. The progress of strain distribution in those cases was similar to specimen S1-1 but slower than S1-1.

4.3.2 Bond stress-slip relationship between PBO-FRCM and concrete

Based on Equations (1) to (3), we can derive the relationship between bond stress and slip of PBO and concrete interface. Figure 4.9a evidences that the bond stress-slip relationship between PBO and concrete at different locations on surface of PBO are similar in case of long bond length. Similar to conventional FRP system (Dai et al. 2005a), it means that bond stress-slip relationship between PBO and concrete in FRCM system is unique regardless of location in case of no slip at free end. Therefore, to simplify and calibrate the bond stress-slip relationship between PBO and concrete more accurately and reliably, we can use the bond stress-slip relationship of first location of each tested specimens due to the fact that observed range of slip is the largest so that the complete bond stress-slip relationship can be observed. Figure 4.9b shows the bond stress-slip relationship for all specimens, each of which is the bond stress-slip relationship at first locations in each specimen. And Figure 4.9c shows the bond stress-slip of ordinary FRP system in a previous study (Dai et al. 2005a). Generally, the shape of bond stress-slip curve in the case of PBO-FRCM

system is similar to that of FRP system. Both of them have two branches: ascending

branch until reaching the maximum bond stress $\bar{\tau}_{max}$, and descending branch ending

at maximum slip corresponding to zero bond stress.
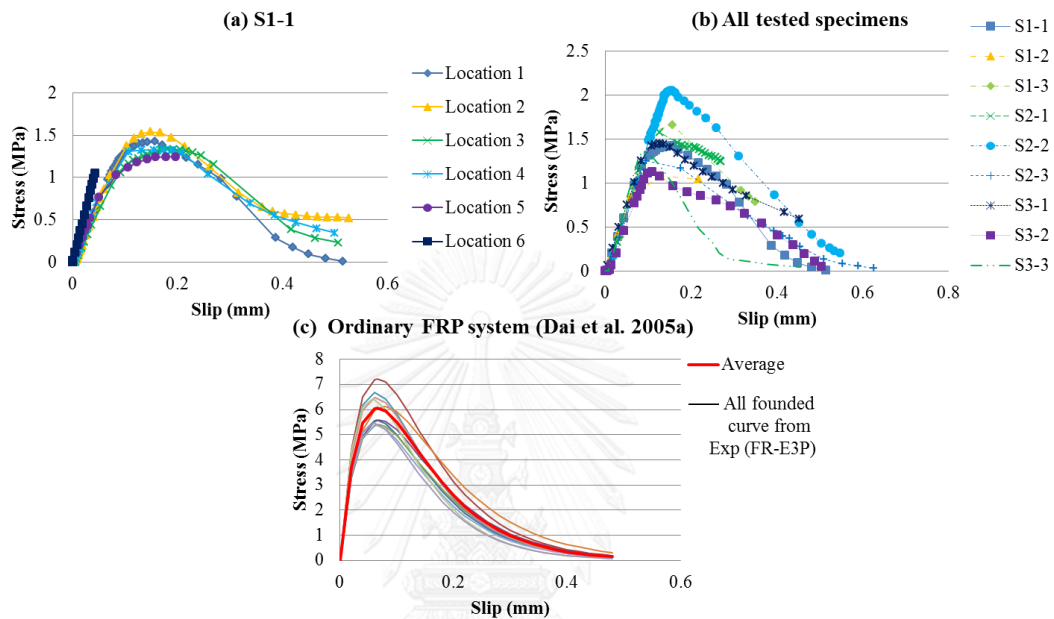
Figure 4. 9 Bond stress-slip relationship between strengthening material and concrete

substrate: (a) specimen S1-1, (b) all tested specimens and (c) ordinary FRP system

(Dai et al. 2005a)

Comparison of transfer load mechanism between PBO-FRCM system with ordinary FRP system

The bond between strengthening materials and concrete is key role for effectiveness

of any external strengthening systems. In fact, the load transfer mechanism between

PBO and concrete in FRCM system is different from the load transfer mechanism

between FRP and concrete in ordinary FRP system. The debonding occurs within surface layer of concrete substrate in most cases of shear test in ordinary FRP system (Figure 4.10a) while the debonding occurs within cementitious layer in many cases of PBO-FRCM system (Figure 4.10b)

(a) Surface of debonding failure of FRP system   (b) Surface of debonding failure of PBO-FRCM system
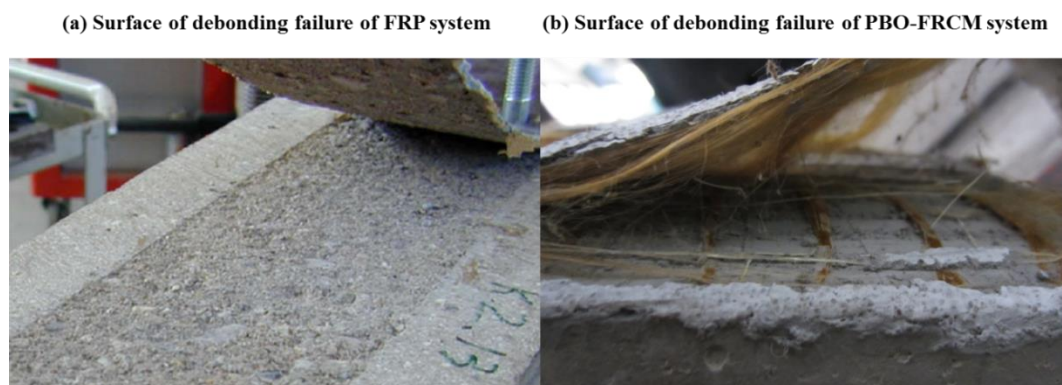
Figure 4. 10 Interface between strengthening material and concrete

4.2.3 Proposed model for bond stress-slip relationship between PBO-FRCM and concrete

For FRP system, many researches on the bond stress-slip relationship between FRP and concrete have been conducted. Based on experimental data, a lot of bond stress-slip curves have been proposed. The bond stress-slip curves include an ascending branch before the maximum bond stress $\bar{\tau}_{max}$ and a descending branch ending at the maximum slip $\bar{s}_f$ corresponding to the zero value of bond stress. Both branches of bond stress-slip curves are nonlinear (Savoia et al. 2003, Wu and Yin 2003, Yuan et al. 2004, Dai et al. 2005a, Wang 2007). To simplify the analysis, some

models adopt linear shapes for both ascending and descending branches (Neubauer and Rostasy 1999, Yao et al. 2005, Wang 2006).

For PBO-FRCM system, the experimental results in this paper evidence that the bond stress-slip relationship has the shape as that of FRP system but difference in some points (Figure 4.9) such as:

- The bond stress-slip relationship has two branches: ascending branch with a greater slope and descending branch with a smaller slope (same characteristics)

- The bond stress-slip relationship has much smaller maximum bond stress, resulting in much smaller fracture energy (different characteristics)

To understand clearly the different mechanism transfer load between FRP system and PBO-FRCM system, we can apply some existing models of FRP system available in literature to PBO-FRCM system. Three local bond-slip models are summarized in Table 4.4 and the debonding force can be obtained by the following equation:

$$P_{max} = \sqrt{2b_f E_f A_f G_f}$$ (6)

Table 4. 4 Existing bond stress-slip model of FRP system

Bond-slip model	$s \leq s_0$	$s > s_0$	τ_{max}	s_0	s_f	β_w
Neubauer and Rostasy (1999)	$\tau_{max}\dfrac{s}{s_0}$	0	$1.8\beta_w f_t$	$0.202\beta_w$		$\sqrt{1.125\dfrac{2-b_f/b_c}{1+b_f/400}}$
Monti et al. (2003)	$\tau_{max}\dfrac{s}{s_0}$	$\tau_{max}\dfrac{s_f-s}{s_f-s_0}$	$1.8\beta_w f_t$	$2.5\tau_{max}\left(\dfrac{t_a}{E_a}-\dfrac{50}{E_c}\right)$	$0.33\beta_w$	$\sqrt{1.5\dfrac{2-b_f/b_c}{1+b_f/100}}$
Dai et al. (2005a)	$\tau = 2BG_f(e^{-Bs}-e^{-2Bs})$	$0.5BG_f$	$\dfrac{0.693}{B}$	$G_f = 0.446\left(\dfrac{G_a}{t_a}\right)^{-0.352}f'^{0.236}_c(E_f t_f)^{0.023}$ $B = 6.846(E_f t_f)^{0.108}(\dfrac{G_a}{t_a})^{0.833}$ $P_{max} = \sqrt{2b_f E_f A_f G_f}$		

where s_0 is slip corresponding to the maximum bond stress τ_{max}

f_t is tensile strength of concrete according to ACI code (ACI-318 2008)

t_a and E_a are the thickness and elastic modulus of cementitious matrix respectively

b_c is the width of concrete prism

β_w is the width ratio factor

s_f is the slip when the bond stress reduces to zero

B is the interfacial ductility index

Table 4. 5 Comparison between calculated results of above existing bond stress-slip models and experimental results

Bond-slip model	Specimens	f'_c (MPa)	$\tau_{max,pre}$ (MPa)	$\dfrac{\tau_{max,pre}}{\tau_{max,exp}}$	$G_{f,pre}$ (N/mm)	$\dfrac{G_{f,pre}}{G_{f,exp}}$
Neubauer and Rostasy (1999)	S1	31	5.33	3.73	0.511	1.48
	S2	41	6.13	5.57	0.588	1.79
	S3	39	5.98	3.46	0.574	1.12
Monti et al. (2003)	S1	31	4.86	3.04	0.705	1.64
	S2	41	5.60	2.73	0.811	1.57
	S3	39	5.46	4.27	0.791	1.74
Dai et al. (2005a)	S1	31	6.34	4.37	0.863	2.28
	S2	41	6.77	5.99	0.921	2.15
	S3	39	6.69	4.96	0.911	2.03

Because the maximum load P_{max} is directly proportional to the square root of interfacial fracture energy G_f regardless of the shape of bond stress-slip curves, a comparison of the pullout bond strength P_{max} is equivalent to a comparison of the interfacial fracture energy. Table 4.5 shows the calculated fracture energy by applying the existing model of FRP system directly to PBO-FRCM system. Because the

existing models of FRP system depend on the compressive strength of substrate concrete f_c', these models are calculated by different compressive strength of concrete for S1, S2 and S3. The values of interfacial fracture energy of these models are higher than the experimental results; approximately 1.4 times for Neubauer and Rostasy's model, 1.6 times for Monti's model and 2.1 times for Dai's model. The values of maximum bond stress of these models are also higher; 2.7 to 6.0 times of the experimental values. Figures 13 show the shapes of existing models that were applied directly on specimen S1-1 compared with the bond stress-slip curves observed in this study. It shows that the curves of existing models of FRP system are not fitting with the experimental results because of the much higher maximum bond stress and much smaller maximum slip at zero bond stress.
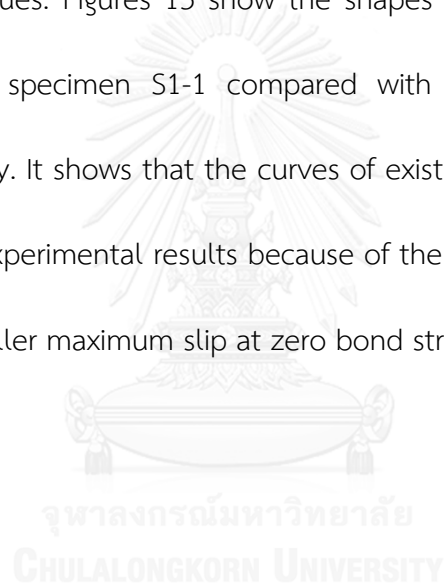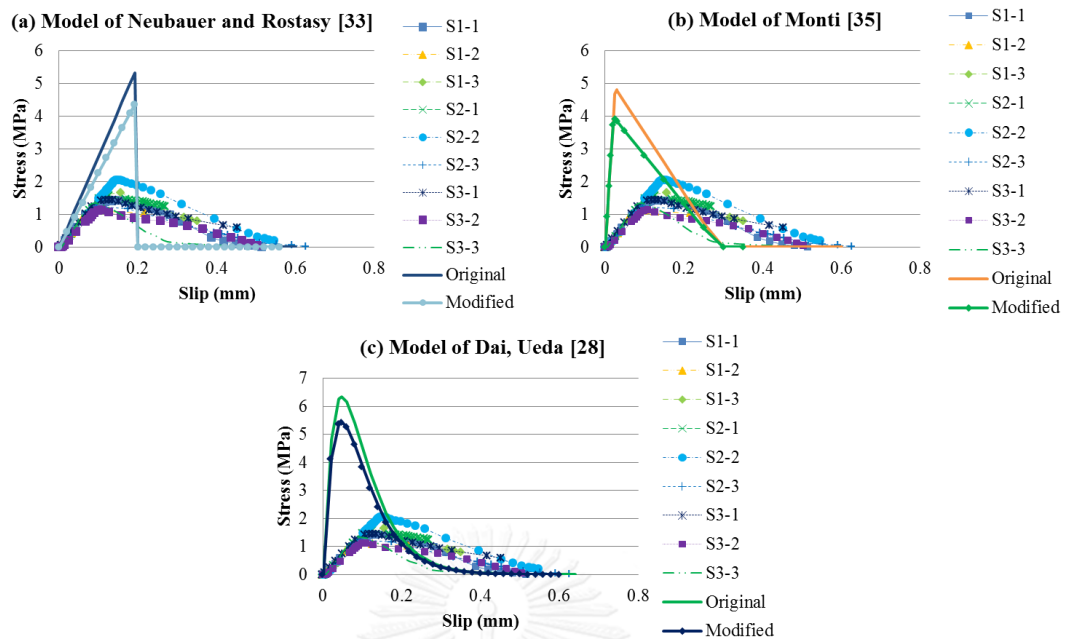
Figure 4. 11 Experimental bond stress-slip curves and existing models curves for

specimens in this study

The reason of those differences between calculated and experimental bond stress-slip curves may be due to the local debonding. In the case of ordinary FRP system, the debonding occurs within substrate concrete layer at the interface between adhesive or primer resin and substrate concrete so that all formula of existing models of FRP system always include significant effect of compressive strength of concrete. However, in case of PBO-FRCM system, the debonding occurs within FRCM layer at interface between PBO mesh and cementitious matrix, therefore the formula for PBO-FRCM system should include the strength of cementitious matrix. As Table 3.1 shows, the strength of cementitious matrix is smaller than that of ordinary concrete which may be the reason of smaller maximum local bond stress and

interfacial fracture energy. Consequently, we can apply existing model by substituting strength of substrate concrete by strength of cementitious matrix. The recalculated results are shown in Figure 4.11 and still very different from the experimental results of this study although they are better than the results that were calculated by applying models of FRP directly. The debonding failure mode of PBO-FRCM shows two debonding surfaces; one is on the FRCM layer side attached on substrate concrete and the other is on the FRCM layer side covering PBO sheet. The thickness of the covering FRCM side is much smaller than the other side that includes the substrate concrete. This condition is quite different from that in ordinary FRP system. Thus only replacing the strength of concrete by the strength of cementitious mortar in formula of existing models is not enough to simulate bond stress-slip of PBO-FRCM system exactly.

However, the mathematical function of Dai's model shows similarity of the experimental curve shape so that we can use and modify this model to simulate bond stress-slip between PBO and concrete. The important parameters of bond stress-slip relationship are: the maximum bond stress (τ_{max}) and corresponding slip; the fracture energy (G_f). The parameters in Table 4.6 are calibrated by the experimental data of maximum bond stress (τ_{max}) and the fracture energy (G_f) shown in Table 4.3. Figure 4. 12 shows obtained best fitting curve with the same

mathematical function as Dai's model based on experimental bond stress-slip curves. The best-fitting curve is in good agreement with the experimental results.

Table 4. 6 Parameters of best-fitting curve of stress-slip based on Dai and Ueda model

G_a (GPa)	G_a/t_a (GPa/mm)	$E_f t_f$ (GPa/mm)	B (mm^{-1})	$G_{f,th}$ (N/mm)	$\tau_{max,th}$ (MPa)	$s_{max,th}$ (mm)	$P_{max,th}$ (kN)
2.603	1.831	12.285	6.831	0.427	1.46	0.101	10.25
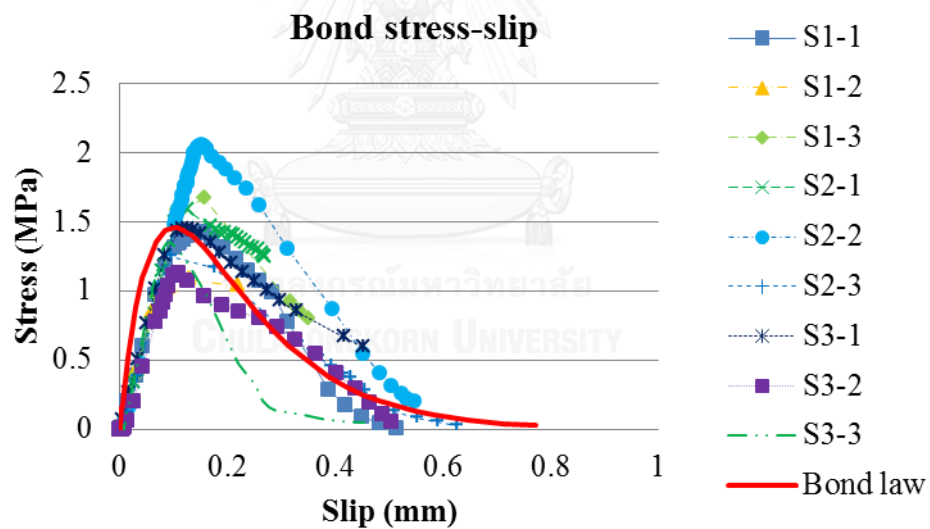
Figure 4. 12 Bond-slip curves between experimental results and best-fitting curve

based on Dai's model

In addition, we can obtain the curves between load and slip at the loaded end of specimens by integrating the strain distribution curves as shown in Figure 4.8. The strain at the loaded end (ε_0) can be obtain by following equation

$$\varepsilon_0 = \frac{P}{E_f A_f} \tag{7}$$

where P is the applied load, and E_f, A_f are the elastic modulus of PBO and area section of PBO, respectively.

Figure 4.13a shows that the load-slip relationship at loaded end of specimens that the bond length is larger than 250 mm in this study and previous study (D'Ambrisi et al. 2012b). The shapes of experimental load-slip curves of both researches are similar, and the average values of maximum load are 10.02 kN for D'Ambrisi's data and 10.21 kN for this study. However, we can see that the ductility of all specimens in this study is higher than the specimens of D'Ambrisi's research because the bond lengths of specimens in this study are longer than those of specimens in previous research. It means that the stage of constant maximum load of this study is longer than that of D'Ambrisi's research. This stage occurred after the applied load had reached proximately to maximum value, the applied load continued to keep constant value while it transferred from loaded end to free end of specimen until debonding occurred. And the initial slope of load-slip curve of each specimen is different as show in Figure 4.13a. In fact, the initial slope of load-slip curve of the

second specimen of previous study (D'Ambrisi 2) is the smallest of all. From the load-slip relationship at loaded end of each specimen, the bond stress-slip curves based on Dai's model can be obtained. The procedure for obtaining local bond stress-slip relationship is presented in the previous study (Dai et al. 2005b). The best fitting curve of experimental load-slip relationship at the load end of specimens S1-1 is shown as in Figure 4.13b. The detailed information of the calculated parameters based on Dai's model is shown in Table 4.7.

Table 4. 7 Calculated parameters of each specimen

Specimens	G_f (N/mm)	B (mm^{-1})	$\tau_{max,th}$ (MPa)	$s_{max,th}$ (mm)
This study				
S1-1	0.345	4.8	0.83	0.144
S1-2	0.328	4.7	0.77	0.147
S1-3	0.514	4.7	1.21	0.147
S2-1	0.429	6.7	1.44	0.103
S2-2	0.517	4.0	1.03	0.173
S2-3	0.455	6.0	1.37	0.113
S3-1	0.378	4.0	0.76	0.173
S3-2	0.429	5.1	1.09	0.136
S3-3	0.447	5.4	1.21	0.128
Average	0.424	5.0	1.07	0.137
D'Ambrisi et al. (2012b)				
Specimen 1	0.461	3.5	0.81	0.198
Specimen 2	0.360	2.7	0.48	0.257
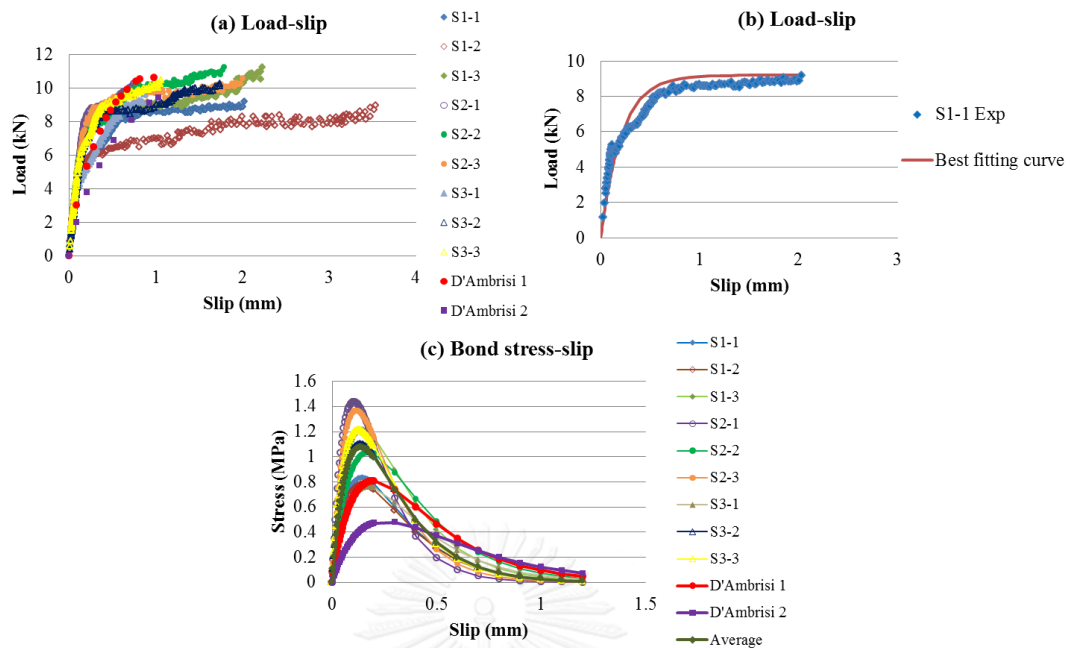
Figure 4. 13 Comparison between experimental data of this study and that of D'Ambrisi

et al. (2012b): (a) Load-slip relationships, (b) Best-fitting curve based on Dai's model

and (c) Stress-slip relationship based on Dai's model

Based on the obtained the best fitting curves of experimental load-slip relationship

at loaded end, we can obtained the bond stress-slip curves using Dai's model as

shown in Figure 4.13c. The calculated maximum bond stresses of this study are

around 0.8 MPa to 1.4 MPa, and the average maximum value is 1.07 MPa while the

calculated maximum of bond stress of D'Ambrisi's data are 0.81 MPa in the first

specimen and 0.48 MPa in the second specimen, and the average maximum value is

0.63 MPa. The calculated values of maximum stress of D'Ambrisi's data in here are

approximately double higher than the calculated values of maximum stress in the

previous study (D'Ambrisi et al. 2012b) because in this study, the bond stresses were

calculated by using b_f for definition of bond surface, while in the previous study

(D'Ambrisi et al. 2012b), they used $2b_f$ for definition of bond surface. Figure 4.13c

also shows that the bond stress-slip curves based on experimental data of this study

are similar to those of D'Ambrisi's data. And the obtained values of maximum bond

stress based on data of this study are higher than those of D'Ambrisi's data. The

reason of differences between results of this study and results of previous study

(D'Ambrisi et al. 2012b) cannot be known at present. We may need more researches

for clarification.

In addition, the obtained bond stress-slip curves based on experimental load-slip

relationship as shown in Figure 4.13c are in rather good agreement with obtained

bond stress-slip curves based on experimental stress-slip relationship as shown in

Figure 4.12. The calculated average value of maximum stress based on experimental

stress-slip as shown in Figure 4.12 is higher than that based on experimental load-slip

as shown in Fig. 4.13c in this study; 1.46 MPa for average value of maximum stress

based on experimental stress-slip relationship and 1.07 MPa for average value of

maximum stress based on experimental load-slip relationship. The reason of

differences between results in Figure 4.12 and results in Figure 4.13c may be due to

the difference in method to take average bond stress-slip behavior and the

difference in configuration of bond stress-slip curve in the experiment and model

mathematical function.

4.4 Summary

Both experimental and analytical programs for investigating the bond between PBO-FRCM system and concrete were conducted in this. The experimental results in this study together with the previous study (D'Ambrisi et al. 2012b) have shown that:

- The experimental results of tested specimens show that the effective bond length of PBO in FRCM systems in this paper is around 250 mm.

- In fact, the load transfer mechanism between PBO and concrete substrate in the case of the FRCM system is different from that between FRP and concrete in the case of the conventional FRP system. The debonding occurs within the substrate concrete surface layer at the interface between adhesive or primer resin layer and substrate concrete in most cases of shear test in the FRP system while the debonding occurs within the cementitious layer at the interface between PBO and cementitious matrix.

- The maximum pullout bond strength P_{max} at debonding slightly directly proportional to the concrete substrate increase.

- The bond stress-slip relationship between PBO and concrete substrate can be represented by a similar mathematical functional model of the conventional FRP system, although the maximum local bond stress and maximum pullout bond strength (fracture energy) are much smaller. The brittleness of the inorganic cementitious matrix (i.e., also the bonding adhesive) seems to be a

reason for the smaller bond strength (fracture energy). Since the factors affecting the bond stress-slip relationship are different from those for conventional FRP systems due to the difference in failure mode, we need more test data to develop a generic model for the PBO-FRCM system, which can calculate not only the bond stress-slip relationship but also the maximum bond strength (fracture energy) and the effective bond length.

- The bond-slip relationship obtained by strain gauge and calibrated by load-slip at the loaded end are in rather good agreement, meaning that the bond stress-slip relationship is unique regardless of the location if the bonded length is long enough.

- The bond stress-slip relationship between PBO and concrete in FRCM systems can be represented by the same mathematical functional model of FRP systems (Dai et al. 2005a).

Chapter 5

Debonding phenomena: Analysis, discussion of test results and proposed model

5.1 General

Debonding phenomenon is an important characteristic to evaluate the effectiveness of any strengthening system and strongly depended on the load transfer mechanisms at the concrete/matrix interface. Because the transfer load mechanism of PBO-FRCM system was different from that of FRP system, so that the process of debonding in PBO-FRCM strengthened RC beams was different than that observed in FRP strengthened RC beams. In fact, the debonding phenomena occurred in the concrete substrate in case of FPR systems and the debonding phenomena occurred within the cementitious matrix with in case of PBO-FRCM system.

There are two main contents in this section: (1) the debonding behavior of strengthened beams with PBO-FRCM system under bending test (2) proposed model for predicting IC debonding for beams strengthened with PBO-FRCM system under flexure load.

5.2 Experimental results

5.2.1 Failure modes

The experimental results of bending test are summarized in Table 5.1

Table 5. 1 Experimental data of applied load

Beam	P_y (kN)	P_u (kN)	δ_u	%	Failure mode
B1-0	54.86	70.63	28.69	0	Flexural
B1-1	56.67	74.70	24.78	5.76	IC debonding
B1-2	64.28	91.85	26.64	30.04	IC debonding
B1-3	69.44	100.61	26.27	42.45	IC debonding
B2-0	53.23	74.23	51.27	0	Flexural
B2-1	62.08	78.23	26.48	5.39	IC debonding
B2-2	67.22	94.88	28.39	27.82	IC debonding
B2-3	70.22	100.02	24.48	34.74	IC debonding
B3-0	53.57	76.61	49.09	0	Flexural
B3-1	61.99	83.12	21.96	8.50	IC debonding
B3-2	66.44	87.50	27.91	14.21	IC debonding
B3-3	71.51	98.70	24.57	28.83	IC debonding

which

P_y and P_u are the load at the yielding tensile steel rebars and the ultimate load on

the beams respectively.

and $\% = \frac{P_u - P_y}{P_u} x 100\%$

The load-mid span deflection experimental curves of all beams in bending test are shown in Figure 5.1. For each curve, there are three straight lines with different slopes corresponding with three stages of beam: un-cracked stage of beam, the stage of beam until yielding steel rebars and the post-yielding steel rebars. The experimental curves showed that the strengthened beams had higher capacities than the controlled beam, but they had smaller deflections than the controlled beam.
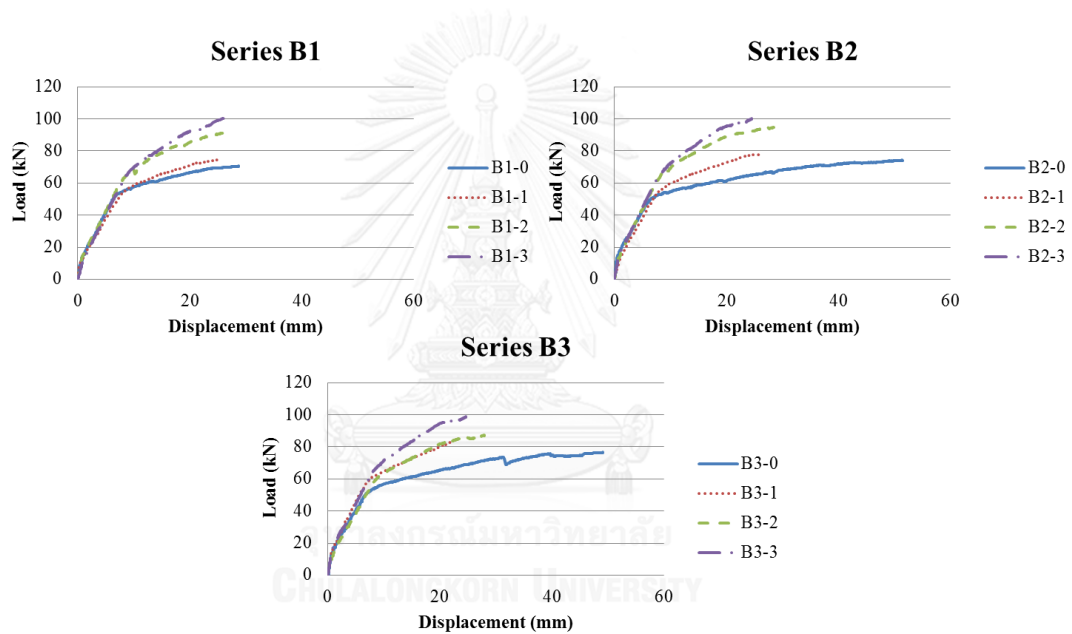
Figure 5. 1 Load-mid span deflection experimental curves in bending test

The yielding loads and ultimate loads of the beams in series B1 are reported in Table 4. In case of the control beam B1-0, the yielding load and ultimate load were 54.86 kN and 70.63kN respectively. The yielding load of the strengthened beam B1-1 was slightly higher than that of the control beam B1-0 and was 56.67 kN. The ultimate load of the beam B1-1 was also higher than that of the control beam B1-0 and was

74.7 **kN**. It's similar to the beam B1-2 and B1-3, both yielding loads and ultimate loads of these beams increased (64.28 **kN** and 91.85 **kN** for beam B1-2; 69.44 **kN** and 100.61 **kN** for beam B1-3, respectively).

In comparison with the control beam B1-0, the ultimate loads of the strengthened beams increased by 5.76 % for the beam B1-1strengthened with one PBO layer, 30.04 for the beam B1-2 strengthened with two PBO layers and 42.45 for the beam B1-3 strengthened with three PBO layers, respectively. It implied that the maximum load capacity of beams was proportion with the number of PBO layers.

The failure mode of the control beam B1-0 was crushing of concrete after yielding tensile steel rebars while IC debonding phenomena occurred in all other beams in series B1 after yielding tensile steel rebars as shown in Figure 5.2 and Figure 5.3. Actually, many vertical cracks appeared in the middle of the strengthened beams and the debonding phenomena initiated in the middle region of the beams that were highest moment region in the beam and then transferring to one of the ends of the strengthened beams. When the debonding reached to the end of the beams, the beams were failed. However, the surface of strengthening material in case of one PBO layer after debonding was different from that in case of two and three PBO layers due to the different of stiffness of strengthening layers as shown as Figure 5.4
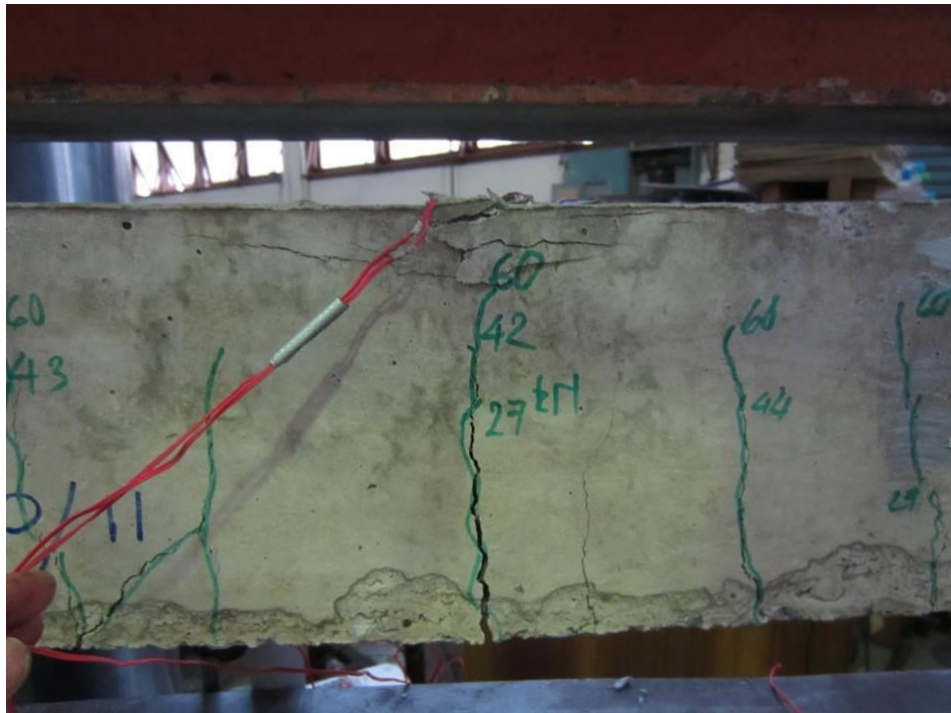
Figure 5. 2 Flexural failure of controlled beam

Figure 5. 3 IC debonding failure of strengthened beams

(a) One PBO layer   **(a) Two and three PBO layer**
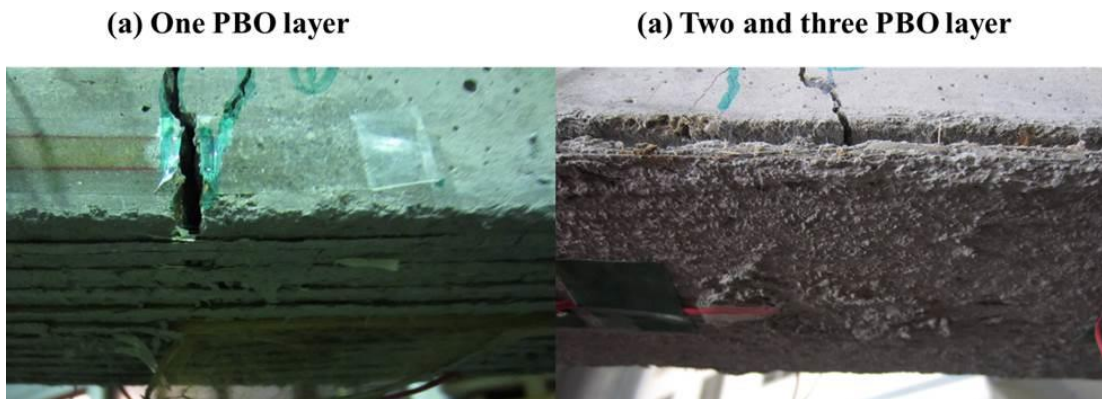
Figure 5. 4 Debonding surface of PBO

The experimental results of the beams in series B2 and series B3 are also reported in Table 5.1. The failure modes of the controlled beam and the strengthened beams in these groups are similar to those in series B1. The controlled beams B2-0 and B23-0 were failed by crushing of concrete after yielding tensile steel rebars. And the failure modes of the strengthened beams were IC debonding failures after yielding tensile steel rebars. The IC debonding phenomena in these groups were the same with those in the series B1.

Both the number of PBO layers and compressive strengths of concrete affected the capacities of beams. However, the experimental results showed that the increase of PBO layers was more effective than the increase of compressive strength of concrete as shown in Figure 5.5. The reason may be due to yielding tensile steel rebars before crushing of concrete in case of the controlled beams and the IC debonding occurred in case of the strengthened beams.
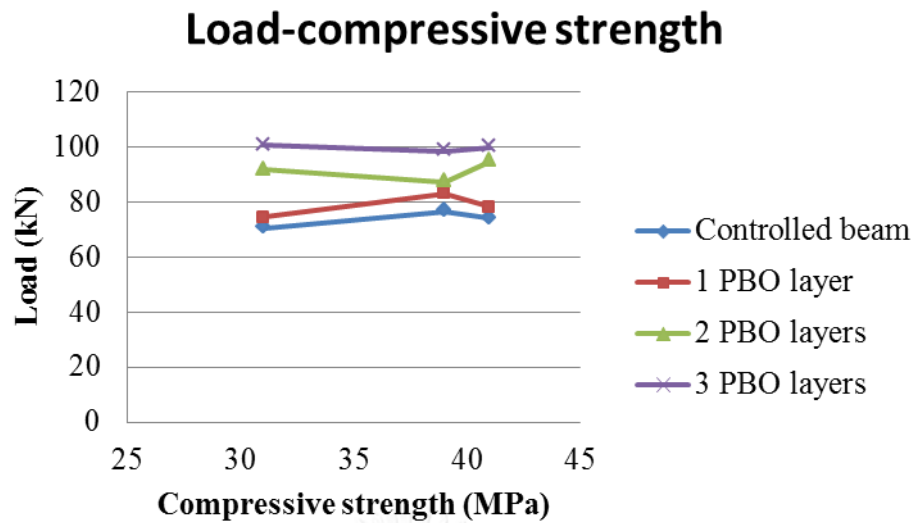
Figure 5. 5 The experimental curves among the compressive strength of concrete,

the number of PBO layers and the capacity of beams

The increase of capacities of beams depended on the number of PBO layers and was

proportion with increase of PBO layers. The IC debonding phenomena occurred in all

the strengthened beams at the interface between concrete and cementitious matrix

with considered slip between PBO and cementitious matrix. In fact, there was an

existing perfect thin layer of cementitious after debonding as shown in Figure 5.6.

Figure 5. 6 The interface between PBO-FRCM and concrete after debonding

5.2.2 Strain distribution

The PBO strain distributions of strengthened beams were similar regardless series of beams. Figure 5.7 showed the measured strains of PBO along the surface of beams of series B1. The highest PBO strains were at location near the middle span where the location of initial debonding was.
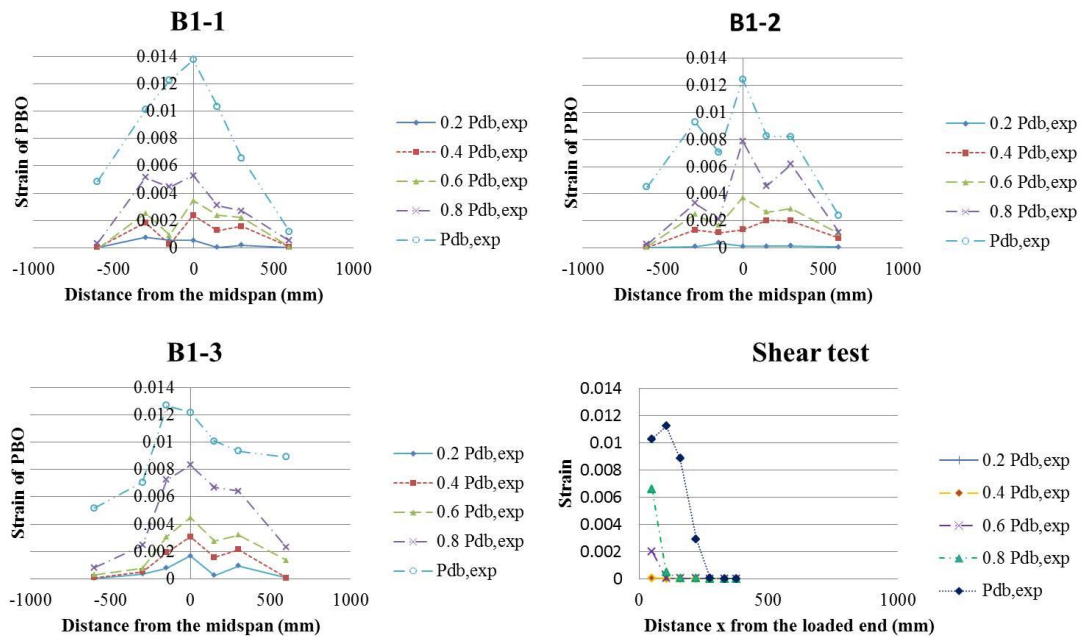
Figure 5. 7 The PBO strain distribution of beams in series B1 and PBO strain distribution in pure shear test

The variation of PBO strains in the strengthened beams was proportional to that of the applied load until reaching the yielding load (around $0.7P_u$); after this value, there was a major change of PBO strains in constant moment zone. It implies that there is a significant transfer of tension forced from the internal tensile steel rebars to external PBO-FRCM system. And based on Figure 5.7, the shape of PBO strain distributions in bending test is the similar to that in shear test. The highest strain is near the middle of beams where the cracks occurred first and decreases toward to the end of beam. However, the effective bond length of PBO in bending test is considered longer than effective bond length in shear test (250 mm). The reason may be due to the effective cracks.

In addition, the strains of compressive concrete, the strains of compressive steel rebars and the strains of tensile steel rebars also were recorded during the test as shown in Figure 5.8. The compressive strains of concrete and steel rebars were negative and tensile strains of PBO and steel rebars were positive.
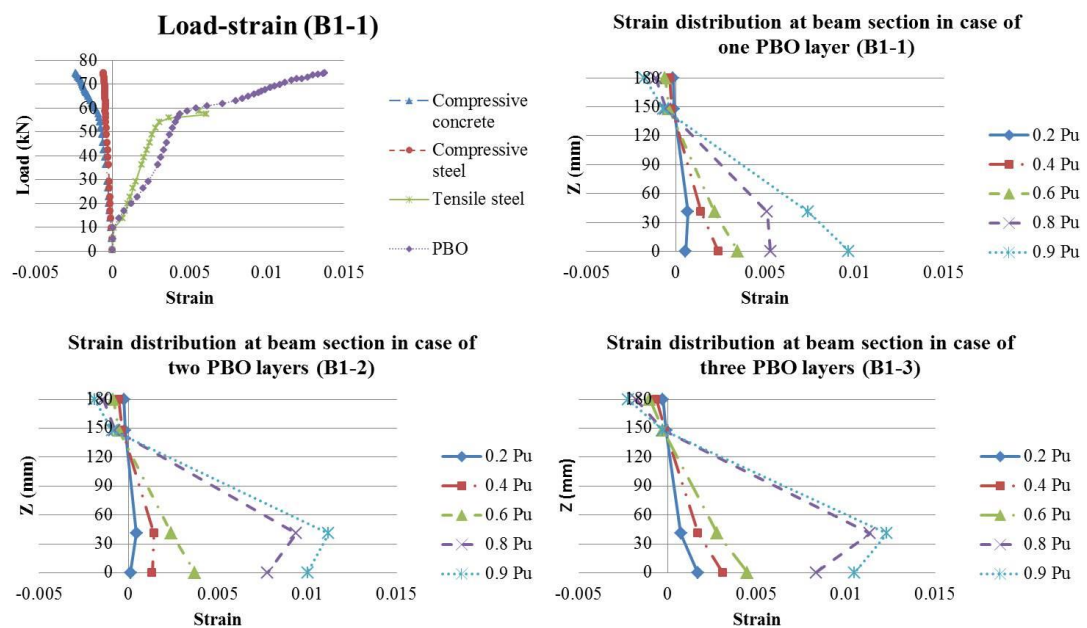
Figure 5. 8 Load-strain curves and strain distribution along the section beam

Based on Figure 5.8, the strains distribution along the depth of section beam were considered approximate to linear until debonding occurred. It implies that the capacity of beam can be calculated by using plain strain of section beam.

5.3 Proposed model for predicting IC debonding

5.3.1 General

Based on experimental results, the strain distribution along the depth of section beam can be considered linear. The results is similar with (*Ombres 2011b),* they confirm

that the structural modelling of PBO-FRCM strengthened beams can used the Bernoulli's hypothesis (perfect bond FRCM to concrete). In fact, tested results evidenced that the slippages between PBO-FRCM system and the concrete substrate were significant only at the collapse of beam

A strain compatibility method is proposed based on the beam deformation theory but including the nonlinear stress-strain relations for steel and compressive concrete, and the linear elastic behavior of the PBO mesh and tensile concrete.

Stress-strain relationship for steel and concrete

The compressive stress-strain relation for concrete is based on the model proposed by Hognestag (Hognestad et al. 1961). The ascending branch is modeled with a parabolic function and descending branch is modeled with a linear function as shown in Figure 5.9

$$For\ 0 \leq \varepsilon_c \leq \varepsilon_0, \qquad f_c = f_c' \left[2\left(\frac{\varepsilon_c}{\varepsilon_0}\right) - \left(\frac{\varepsilon_c}{\varepsilon_0}\right)^2 \right]; \quad \varepsilon_0 = \frac{2f_c'}{E_c} \qquad (8)$$

$$For\ \varepsilon_0 \leq \varepsilon_c, \qquad f_c = f_c'[1 - k(\varepsilon_c - \varepsilon_0)]; \quad k = \frac{0.15}{0.0035 - \varepsilon_0}$$

where ε_c is train in the concrete at any particular point, f_c is stress in the concrete corresponding to ε_c, f_c' is maximum compressive stress, ε_0 is strain corresponding to f_c'
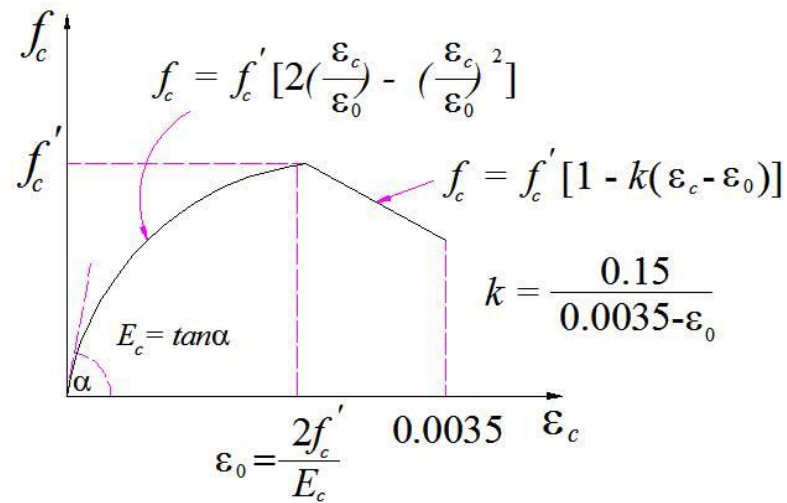
Figure 5. 9 Stress-strain curve of compressive concrete

The stress-strain relationship of the steel can be modeled by elastic perfectly plastic

curve in tension and compression as shown in Figure 5.10

$$For\ \varepsilon_s \leq \varepsilon_y, \qquad\qquad f_s = E_s \varepsilon_s$$

$$For\ \varepsilon_y < \varepsilon_s \leq \varepsilon_{rupt}, \qquad f_s = f_y \qquad\qquad (9)$$

$$For\ \varepsilon_s > \varepsilon_{rupt}, \qquad\qquad f_s = 0$$

where ε_s is steel strain at a particular point, f_s is stress in steel at ε_s, f_y is yielding

stress of the steel, ε_{rupt} is strain at failure
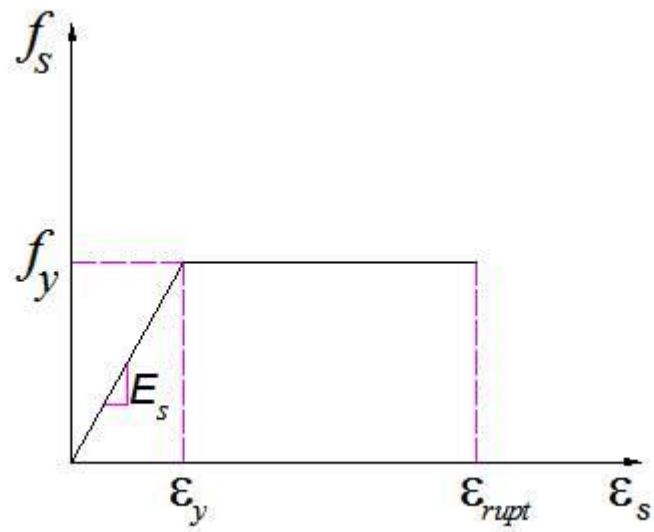
Figure 5. 10 Stress-strain curve of steel rebars

Stress-strain relationship for PBO mesh

A simplification can be achieved by assuming that the contribution of transverse

mechanical properties is negligible as shown in Figure 5.11

$$\sigma_f = E_f \varepsilon_f \tag{10}$$

E_f is the elastic modulus of PBO, ε_f is strain of PBO and ε_{fu} is the ultimate strain of

PBO
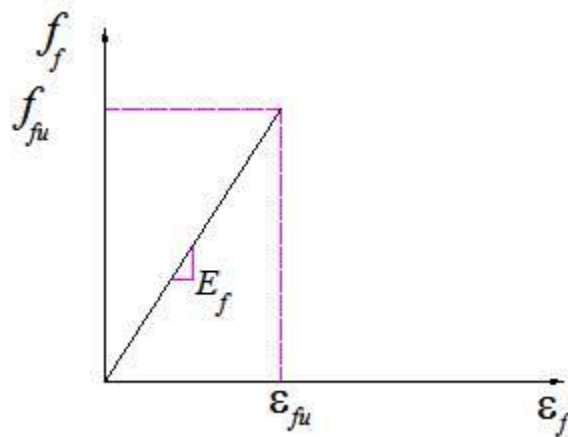
Figure 5. 11 Stress-strain curve of PBO

Based on the strain compatibility and equilibrium of internal forces, PBO stress or external load can be predicted for a specific loading stage. In view of nonlinear behavior of concrete and reinforcing steel, this analysis should be performed by an iterative procedure as shown in Figure 5.12. However, this section analysis can be used to predict in cases of the crushing of concrete and rupture of PBO mesh. It needs to supplement a criteria debonding in order to can be predict debonding phenomena occurred in beam.

Start

Input the geometry of the PBO strengthened beam, the properties of materials, and load P

$\varepsilon_f = 0$

$\varepsilon_f = \varepsilon_f + \varepsilon_{fu} / 10000$

$h_n = d_2 + h / 10000$

Considering that $\varepsilon_c \leq \varepsilon_{co}$

Considering that steel bars are not yielding

The moment attained by the section analysis approximates the external moment, steel aren't yielding & $\varepsilon_c \leq \varepsilon_{co}$

Yes → End

Considering that only lower steel bars are yielding

$h_n < h$

The moment attained by the section analysis approximates the external moment, only lower bars are yielding& $\varepsilon_c \leq \varepsilon_{co}$

Yes → End

Considering that all steel bars are yielding

The moment attained by the section analysis approximates the external moment, all bars are yielding & $\varepsilon_c \leq \varepsilon_{co}$

Yes → End

Considering that $\varepsilon_{cu} \geq \varepsilon_c > \varepsilon_{co}$

Considering that steel bars are not yielding

The moment attained by the section analysis approximates the external moment, bars aren't yielding & $\varepsilon_{cu} \geq \varepsilon_c > \varepsilon_{co}$

Yes → End

Considering that only lower steel bars are yielding

The moment attained by the section analysis approximates the external moment, lower bars're yielding & $\varepsilon_{cu} \geq \varepsilon_c > \varepsilon_{co}$

Yes → End

Considering that all steel bars are yielding

The moment attained by the section analysis approximates the external moment, all bars are yielding & $\varepsilon_{cu} \geq \varepsilon_c > \varepsilon_{co}$

Yes → End

$h_n = h_n + h / 10000$

Figure 5. 12 Flow chat for calculating PBO stress for a given load

5.3.2 Criteria debonding

A similar approach based on (Zhang et al. 2011), for a PBO-FRCM strengthened beam, the debonding failure is estimated by evaluating maximum transferred shear forced between the PBO and concrete. A general case of beam under four-point bending load is analysed. The debonding process in different locations such as shear flexure zone (Zone I) and constant moment zone (Zone II) as shown in Figure 5.13
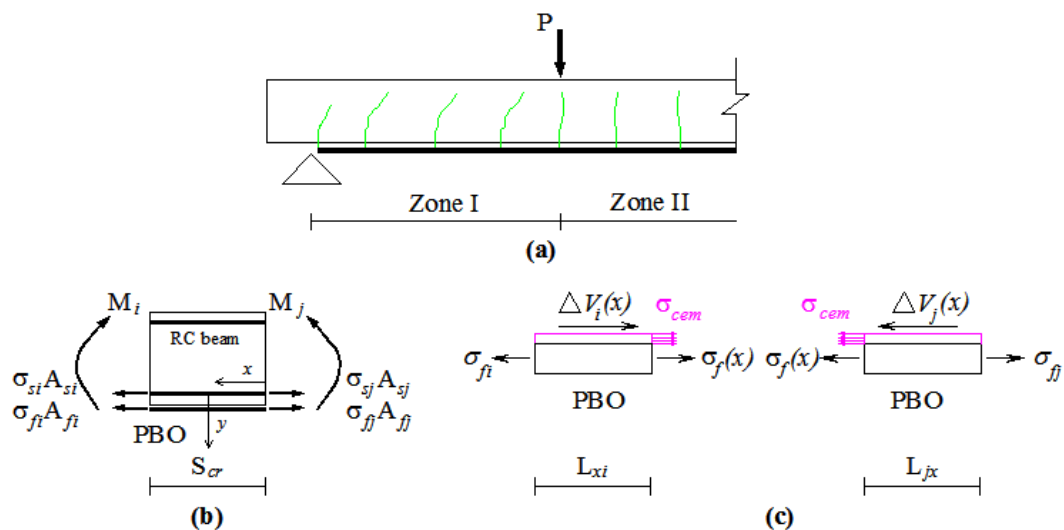
Figure 5. 13 (a) Illustration of zone distribution, (b) An example element and (c) Shear transfer in PBO-FRCM

The transfer shear force within a longitudinal bonded distance x from crack end j can be expressed as

$$\Delta V_{j(x)} = b \int_0^x \tau_{j(x)} dx = A_f\left(\sigma_{fj} - \sigma_{f(x)}\right) - b \int_0^{t_{cem}} \sigma_{cem} dy \tag{11}$$

where σ_{fj} is stress of PBO at the crack j, S_{cr} is the crack spacing of beam

t_{cem} and σ_{cem} are the thickness and tensile strength of cementitious matrix, respectively

The local transfer shear stresses between the FRCM and concrete depend on the relative displacement between both materials through the constitutive behavior of the interface by using local bond slip relationship. The PBO stress is highest at the location of crack and decrease with the increase of distance from the crack and it becomes zero at the zero-slip point where the slip between FRCM and concrete is zero. Therefore, the transfer shear be calculated by followings:

-For the case of constant moment zone

$$\Delta V_{oi} = \Delta V_{jo} = A_f E_f \left(\varepsilon_{fi} - \varepsilon_{fo} \right) - t_{cem} b f_{cem} \tag{12}$$

And $L_{oi} = L_{jo} = \frac{S_{cr}}{2}$ \hfill (13)

- For the shear flexure zone

$$\Delta V_{oi} = A_f E_f (\varepsilon_{fi} - \varepsilon_{fo}) \tag{14}$$

$$\Delta V_{jo} = A_f E_f (\varepsilon_{fj} - \varepsilon_{fo}) \tag{15}$$

And $\frac{L_{oi}}{L_{jo}} = \frac{M_i}{M_j}$ \hfill (16)

In case of this study, the beams were tested under four-point bending condition and the experimental results showed that IC debonding phenomena occurred in all

specimens. So that, it will be enough to analyze the element at constant moment zone, because the bending moment is highest value in comparison with remaining sections. And based on the strain compatibility, the PBO stress at crack section and zero-slip section can be calculated as shown in Figure 5.14 and Figure 5.15
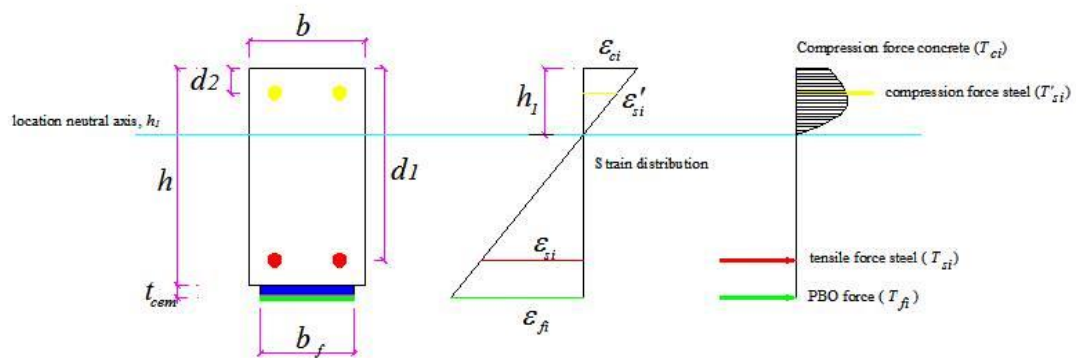

Figure 5. 14 Stress and strain distribution after formation of crack in concrete at crack section
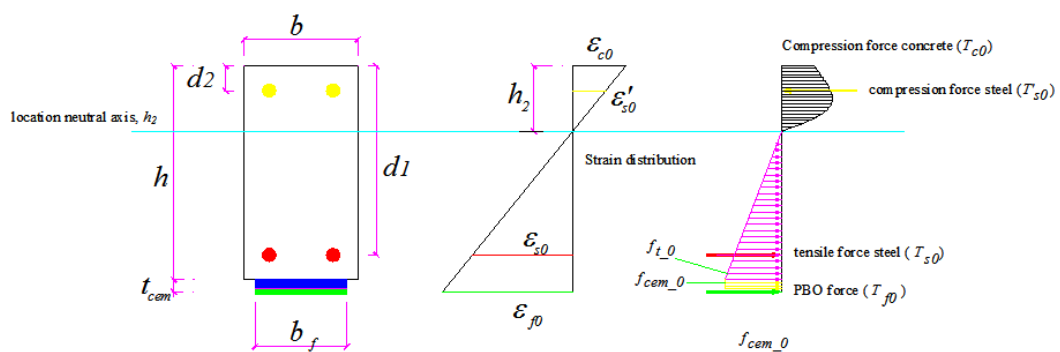
Figure 5. 15 Stress and strain distribution after formation of crack in concrete at zero-slip section

Based on (Zhang et al. 2011),the criteria debonding for PBO-FRCM strengthened RC beam can be written as follows:

$$\begin{cases} V_{trans} \geq V_{max} & \rightarrow & debonding \\ V_{trans} < V_{max} & \rightarrow & no\ debonding \end{cases} \tag{17}$$

which

V_{trans} is transfer shear force in beams and calculated by:

$$V_{trans} = \Delta V_{oi} = \Delta V_{jo} = A_f E_f (\varepsilon_{fi} - \varepsilon_{fo}) - t_{cem} b f_{cem} \tag{18}$$

At zero-slip section, we can assume that:

$$f_{t\_0} = f_{cem\_0} = 0.35 f_{cem\_u} \tag{19}$$

ε_{fi} and ε_{f0} are the PBO stress at the crack section and zero-slip section respectively

and are calculated based on strain compatibility of section beam as shown in Figure

5.14 and Figure 5.15

V_{max} is the maximum bond strength of PBO-FRCM in bending test and calculated

by:

$$V_{max} = \begin{cases} P_{max} & L \geq 250mm \\ \alpha P_{max1} & L < 250mm \end{cases} \tag{20}$$

where L is the bond length of PBO

P_{max} is the maximum bond strength of PBO-FRCM in pure shear test

$$P_{max} = \sqrt{2 b_f A_f E_f G_f} \tag{21}$$

G_f is the fracture energy when debonding occurs in shear test and $G_f = 0.424 \left(\frac{N}{mm}\right)$

b_f and E_f are the width and elastic modulus of PBO respectively

$A_f = n_f b_f t_f$ is the area of PBO layers; n_f and t_f are the number thickness of PBO.

$$\alpha = \begin{cases} \sin\left(\frac{\pi}{2}\frac{L}{250}\right) & L \leq 250 \ mm \\ 1 & L > 250 \ mm \end{cases} \tag{22}$$

Table 5. 2 Calculated results based on Proposed model

Specimen	Number of layer	Crack spacing	$L(mm)$	α	V_{max}	P_{pre}	V_{trans}	$P_{db,exp}$	$\%\Delta P_{db}$
B1-1	1	89	44.5	0.276	2.82	61.26	2.82	74.7	17.99
B1-2	2	80	40	0.249	3.59	73.33	3.59	91.85	20.16
B1-3	3	74	37	0.230	4.07	99.78	4.07	100.61	0.82
B2-1	1	80	40	0.249	2.54	61.49	2.54	78.24	21.41
B2-2	2	75	32.5	0.233	3.19	70.24	3.19	94.88	25.97
B2-3	3	72	36	0.224	4.30	99.95	4.30	100.02	0.07
B3-1	1	78	39	0.243	2.48	61.32	2.48	83.12	26.23
B3-2	2	74	37	0.230	3.32	68.86	3.32	87.50	21.30
B3-3	3	72	36	0.224	3.96	98.48	3.96	98.70	0.22
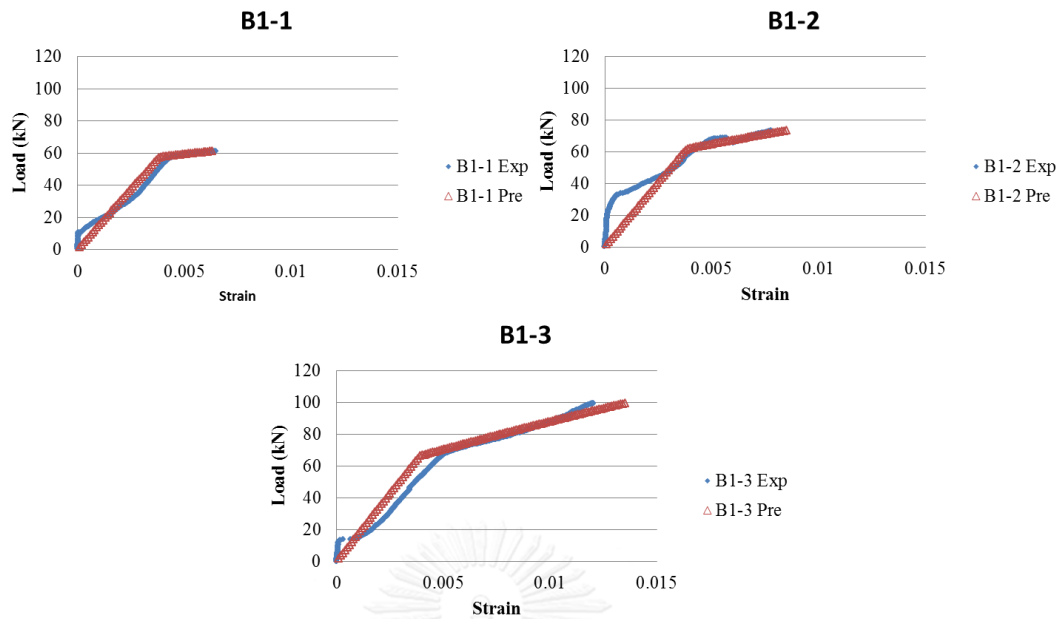
Figure 5. 16 Comparison of PBO strain between predicted results and experimatal data until P_{pre}

Figure 5.17 show that the predicted PBO strains are rather good with experimental PBO strains until P_{pre}. It implies that the model describes the behavior of tested beams is close with experimental behavior of tested beam until the value of P_{pre}.

The calculated results based on proposed model are reported in Table 5.2. All predicted failures are debonding failures. The predicted results are rather good agreement with experimental results. The deviation between predicted load and experimental data is around less than 25% as shown in Figure 5.17
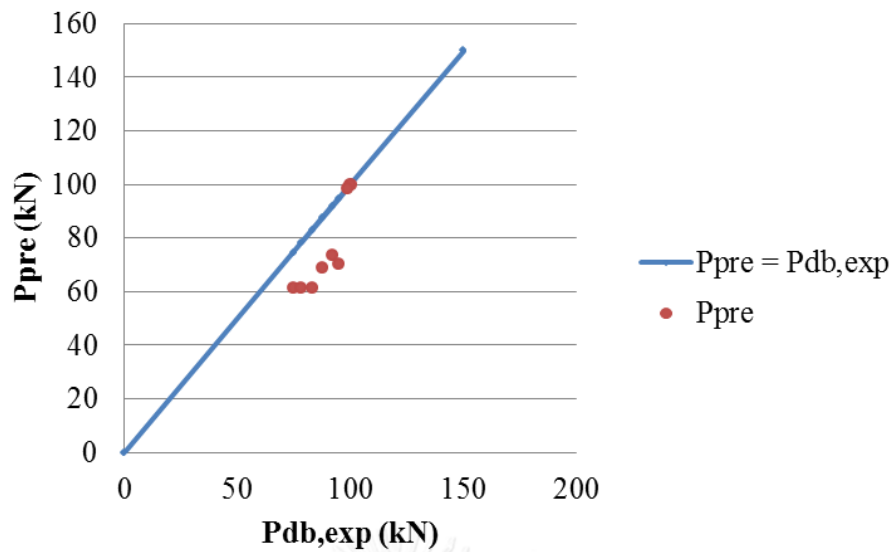
Figure 5. 17 Comparison between calculated results based on proposed model and

experimental results

All the calculated results are lower than experimental data. The first reason, as above mentioned, because there are many cracks occurred in beams in test, so that it will make the transfer mechanical between FRCM and concrete in bending test differently than that in shear test. In fact, the effective bond lengths of PBO in bending tests were longer than effective bond length of PBO in shear tests (250 mm) as shown in Figure 5.7. Therefore, the maximum bond strength of PBO-FRCM in bending test (V_{max}) may be higher than maximum bond strength of PBO-FRCM in pure shear test (P_{max}). The second reason may be due to the measured crack spacing because the cracks spacing is very complicated and depend on the constitutive concrete and distribution of coarse in concrete. In here, the

experimental data of cracks spacing is average values and they are rather small than crack spacing in previous research (Zhang et al. 2011).

5.4 Summary

The debonding of PBO-FRCM was investigated in this study involving with the effectiveness of compressive strength of concrete and the number of PBO layer. The experimental results and analysis in this study have shown that:

- The capacities of strengthened beams are directly proportional to the increasing of the number of PBO layers.

- The load transfer mechanism between PBO-FRCM and concrete in bending test is similar to that in pure shear test. However, based on the experimental results, maybe the effective bond length of PBO in bending test is longer than that in shear test due to cracks. We need more test to develop a generic model for the PBO-FRCM system, which can be calculated bond-slip relationship and effective bond length only in shear test but also in bending test.

- The increasing of compressive strength of concrete in this study affects slightly on the capacity of beams.

- The debonding phenomenon of PBO-FRCM strengthening system is different from that of FRP strengthening system. The debonding occurs within

cementitious matrix in case of PBO-FRCM system while the debonding occurs in concrete substrate in case of FRP system.

- The strain distribution of materials along depth of section beam can be considered linear before debonding occurs. In fact, the experimental results show that the slip between PBO-FRCM and concrete are only significant when debonding occurs.

- The behavior of IC debonding in PBO-FRCM strengthened RC beams can be predicted based on strain plain compatibility of section beam and criteria debonding that modified from the model of FRP system. And the calculated results of proposed model are rather good agreement in comparison with experimental data (around less than 25%)

Chapter 6

Conclusions and recommendations

6.1 General

The experimental and the analytical program reported in this thesis have provided an understanding of the debonding behavior of PBO-FRCM externally bonded PBO mesh for flexural strengthening of RC beams. The main objectives of this study: (1) the effective bond length of PBO mesh for PBO-FRCM system, (2) the bond slip law between PBO mesh and concrete, (3) the intermediate crack induced debonding (IC debonding) behavior of PBO-FRCM strengthened RC beams under bending load, and (4) proposed model for predicting IC debonding for beams strengthened with PBO-FRCM under flexural condition. The following sections highlight the conclusions that can be drawn based on the investigation of this study. The conclusions from the experimental results and analytical study are reported in this section. The recommendations for future wok are also proposed.

6.2 Effective bond length of PBO and bond stress-slip relationship between PBO-FRCM and concrete

Both experimental and analytical programs for investigating the bond between PBO-FRCM system and concrete were conducted in this. The experimental results in this study together with the previous study (D'Ambrisi et al. 2012b) have shown that:

- The experimental results of tested specimens show that the effective bond length of PBO in FRCM systems in this paper is around 250 mm.

- In fact, the load transfer mechanism between PBO and concrete substrate in the case of the FRCM system is different from that between FRP and concrete in the case of the conventional FRP system. The debonding occurs within the substrate concrete surface layer at the interface between adhesive or primer resin layer and substrate concrete in most cases of shear test in the FRP system while the debonding occurs within the cementitious layer at the interface between PBO and cementitious matrix.

- The maximum pullout bond strength P_{max} at debonding slightly directly proportional to the concrete substrate increase.

- The bond stress-slip relationship between PBO and concrete substrate can be represented by a similar mathematical functional model of the conventional FRP system, although the maximum local bond stress and maximum pullout bond strength (fracture energy) are much smaller. The brittleness of the inorganic cementitious matrix (i.e., also the bonding adhesive) seems to be a reason for the smaller bond strength (fracture energy). Since the factors affecting the bond stress-slip relationship are different from those for conventional FRP systems due to the difference in failure mode, we need more test data to develop a generic model for the PBO-FRCM system, which

can calculate not only the bond stress-slip relationship but also the maximum bond strength (fracture energy) and the effective bond length.

- The bond-slip relationship obtained by strain gauge and calibrated by load-slip at the loaded end are in rather good agreement, meaning that the bond stress-slip relationship is unique regardless of the location if the bonded length is long enough.

- The bond stress-slip relationship between PBO and concrete in FRCM systems can be represented by the same mathematical functional model of FRP systems (Dai et al. 2005a).

6.3 IC debonding behavior of externally bonded PBO mesh for flexural strengthening of RC beam and proposed model for predicting IC debonding

The debonding of PBO-FRCM was investigated in this study involving with the effectiveness of compressive strength of concrete and the number of PBO layer. The experimental results and analysis in this study have shown that:

- The capacities of strengthened beams are directly proportional to the increasing of the number of PBO layers.

- The load transfer mechanism between PBO-FRCM and concrete in bending test is similar to that in pure shear test. However, based on the experimental results, maybe the effective bond length of PBO in bending test is longer than that in shear test due to cracks. We need more test to develop a generic model for the PBO-FRCM system, which can be calculated bond-slip

relationship and effective bond length only in shear test but also in bending test.

- The increasing of compressive strength of concrete in this study affects slightly on the capacity of beams.

- The debonding phenomenon of PBO-FRCM strengthening system is different from that of FRP strengthening system. The debonding occurs within cementitious matrix in case of PBO-FRCM system while the debonding occurs in concrete substrate in case of FRP system.

- The strain distribution of materials along depth of section beam can be considered linear before debonding occurs. In fact, the experimental results show that the slip between PBO-FRCM and concrete are only significant when debonding occurs.

- The behavior of IC debonding in PBO-FRCM strengthened RC beams can be predicted based on strain plain compatibility of section beam and criteria debonding that modified from the model of FRP system. And the calculated results of proposed model are rather good agreement in comparison with experimental data (around less than 25%)

6.3 Recommendation for future work

Based on achieved the objectives of this study, more investigations are necessary to understand about the debonding behavior of concrete structures strengthened with PBO-FRCM system fully. Some recommendations can be considered for future work:

- Investigation on the effective bond length of PBO in shear test in case of multi PBO layers in shear test

- Applying finite element method to predict bond stress-slip between PBO-FRCM and concrete

- Applying finite element method to predict IC debonding of RC beams strengthened with PBO-FRCM

- Investigation on the PBO-FRCM strengthening shear of concrete structures

- Investigation on the PBO-FRCM strengthening concrete structures under severe environmental conditions such as high temperature, fire, salt attack …

The effect of applied loads on the concrete structures strengthening with PBO-FRCM system should be considered such as fatigue load, seism

LIST OF PUPLICATIONS

Submitted

C.T.M.Tran, B. Stitmannaithum, T. Ueda "INVESTIGATION ON THE BOND BEHAVIOUR BETWEEN PBO-FRCM STRENGTHENING MATERIAL AND CONCRETE", Proceeding of the 6th ACEC and the 6th AEEC, November 2013, Bangkok, Thailand.

C.T.M.Tran, B. Stitmannaithum, T. Ueda "INVESTIGATION OF THE BOND BEHAVIOUR BETWEEN PBO-FRCM STRENGTHENING MATERIAL AND CONCRETE", Journal of Advanced concrete Technology. It was accepted on 2014-12-09

B. Stitmannaithum, T. Ueda, C.T.M.Tran "INVESTIGATION ON THE DEBONDING PHENOMENA OF PBO-FRCM STREGNTHENING SYSTEM IN FLEXURALLY STRENGTHENDED REINFORCED CONCRETE BEAMS", the Fifth International Conference on Construction Materials, ConMat'15, Canada.

Plan to submit soon

C.T.M.Tran, B. Stitmannaithum, T. Ueda " IC DEBONDING BETWEEN PBO-FRCM STRENGTHENING MATERIAL AND CONCRETE IN FLEXURALLY STRENGTHENED RC BEAM"

REFERENCES

A. Bruckner, R. O., M. Curbach, (2005). "Textile reinforced concrete for strengthening in bending and shear." *Materials and structures*, 39, 741-748.

ACI-318, (2008). Building Code Requirements for Structural Concrete and Commentary.

ACI-440.2R, (2008). Guide for the design and construction of externally bonded FRP system for strengthening concrete structures.

Bisby, L., Stratford, T., Smith, J. and Halpin, S., (2011). "FRP versus fiber reinforced cementitious mortar systems at elevated temperature." *American Concrete Institute*.

Chen, J. F. and Teng, J. G., (2001). "Anchorage strength models for FRP and steel plates bonded to concrete." *Journal of Structural Engineering*, 127(7), 784-791.

D'Ambrisi, A., Feo, L. and Focacci, F., (2012a). "Bond-slip relations for PBO-FRCM materials externally bonded to concrete." *Composites Part B: Engineering*, 43(8), 2938-2949.

D'Ambrisi, A., Feo, L. and Focacci, F., (2012b). "Experimental analysis on bond between PBO-FRCM strengthening materials and concrete." *Composites Part B: Engineering*, 44(1), 524-532.

D'Ambrisi, A., Feo, L. and Focacci, F., (2013). "Experimental and analytical investigation on bond between Carbon-FRCM materials and masonry." *Composites Part B: Engineering*, 46, 15-20.

Dai, J., Ueda, T. and Sato, Y., (2005a). "Development of the Nonlinear Bond Stress-Slip Model of Fiber Reinforced Plastics Sheet-Concrete Interfaces with a Simple Method." *Journal of Composites for Construction*, 9(1), 52-62.

Dai, J., Ueda, T. and Sato, Y., (2005b). "Unified Analytical Approaches for Determining Shear Bond Characteristics of FRP-Concrete Interfaces through Pullout Tests." *Journal of Advanced Concrete Technology*, 4(1), 133-135.

HB-305, (2008). Design handbook for RC structures retrofitted with FRP and meta plates: beams and slabs. Standards Australia.

Hognestad, E., Hanson, N. W. and McHenry, D., (1961). "Concrete stress distribution in ultimate strength design." *ACI Structural Journal*, 57(2).

Hosseini, A. and Mostofinejad, D., (2014). "Effective Bond Length of FRP-to-Concrete Adhesively-Bonded Joints: Experimental Evaluation of Existing Models." *International Journal of Adhesion & Adhesives*, 48, 150-158.

Monti, G., Renzelli, M. and Luciani, P., (2003). "FRP Adhesion in Uncracked and Cracked Concrete Zones". *Proceedings of the Sixth International Symposium on FRP Reinforcement for Concrete Structures (FRPRCS-6)*, Singapore.

Neubauer, U. and Rostasy, F. S., (1999). "Bond Failure of Concrete Fiber Reinforced Polymer Plates at Inclined Cracks-Experiments and Fracture Mechanics Model". *Proceeding 4th International Symposium FRP Reinforcement for RC Structures*, Edinburgh, Scotland.

Ohama, Y., (1995). *Handbook of polymer-modified concrete and mortars*. United states of America, Noyes Publications.

Ombres, L., (2009). "Structural performance of reinforced concrete beams strengthened with PBO fibre reinforced cementitious mortar." *Concrete solutions-Grantham, Majorana & Salomoni (Eds)*, 363-367.

Ombres, L., (2011a). "Debonding analysis of reinforced concrete beams strengthened with fiber reinforced cementitious mortar." *Engineering Fracture Mechanics*, 81, 94-109.

Ombres, L., (2011b). "Flexural analysis of reinforced concrete beams strengthened with a cement based high strength composite material." *Composite Structures*, 94(1), 143-155.

Ruredil, T. D. o., (2006). Ultra high mechanical performance Polyparaphenylene benzobisoxazole (PBO) fibre mesh, with a stabilised inorganic matrix, for structural reinforcement of concrete. Report.

Savoia, M., Ferracuti, B. and Mazzotti, D., (2003). "Non linear bond-slip law for FRP-concrete interface". *Proceeding of the 6th International Symposium on FRPRCS, Singapore*.

Seracino, R., Saifulnaz, M. R. R. and Oehlers, D. J., (2007). "Generic Debonding Resistance of EB and NSM Plate-to-Concrete Joints." *Journal of Composites for Construction*, 11(1), 62-70.

Taljsten, B. and Blanksvard, T., (2007). "Mineral based bonding of CFRP to strengthen concrete structures." *Journal of Composites for Constructions, ASCE*, 11(2), 120-128.

Taljsten, B. and Blanksvard, T., (2008). "Strengthening of concrete structures with cement based bonded composites." *Nordic Concrete Federation*, 2, 38, 133-153.

Tommaso, A. D., Focacci, F. and Mantegazza, G., (2008). "PBO-FRCM composites to strengthen RC beams: mechanics of adhesion and efficiency". *Fourth International conference on FRC Composites in Civil Engineering (CICE 2008)*.

Tommaso, A. D., Focacci, F., Mantegazza, G. and Gatti, A., (2007). "FRCM versus FRP composites to strengthen RC beams: A comparative analysis". *Proceedings of the international Symposium on Fibre Reinforced Polymers Reinforced Concrete Structures, FRPRCS-8, Patras, Greece*.

Toutanji, H. and Deng, Y., (2007). "Comparison between Organic and Inorganic Matrices for RC Beams Strengthened with Carbon Fiber Sheets." *Journal of Composites for Construction*, 11(5), 507-513.

Toutanji, H., Zhao, L. and Zhang, Y., (2006). "Flexural behavior of reinforced concrete beams externally strengthened with CFRP sheets bonded with an inorganic matrix." *Engineering Structures*, 28, 557-566.

Triantafillou, T. C. and Papanicolaou, C. G., (2006). "Shear strengthening of reinforced concrete members with textile reinforced mortar jackets." *Mat & Struct*, 39(1), 93-103.

Wang, J., (2006). "Non linear bond-slip analysis of delamination failure of FRP reinforced concrete beam-Part I: Closed-form solution." *International Journal of Solids and Structures*, 43(21), 6649-6664.

Wang, J., (2007). "Cohesive-bridging zone model of FRP-concrete interface debonding." *Engineering Fracture Mechanics*, 74, 2643-2658.

Wu, H. C. and J.Teng, (2002). "*Innovative cement based thin sheet composites for retrofit*." *Proceedings of the third international composite conference for infrastructures, San Francisco, CA*

Wu, H. C. and Sun, P., (2005). "Fiber reinforced cement based composite sheets for structural retrofit.". *Proceedings of the International Symposium on Bond Behaviour of FRP in Structures (BBFS 2005)*.

Wu, Z. and Yin, J., (2003). "Fracture behaviors of FRP-strengthened concrete structures." *Engineering Fracture Mechanics*, 70(10), 1339-1355.

Wu, Z. S., Iwashita, K., Hayashi, K., Higuchi, T., Murakami, S. and Koseki, Y., (2003). "Strengthening Prestressed-concrete Girders with Externally Prestressed PBO Fiber Reinforced Polymer Sheets." *Journal of Reinforced Plastics and Composites*, 22(14), 1269-1286.

Yao, J., Teng, J. G. and Chen, J. F., (2005). "Experimental study on FRP-to-concrete bonded joints." *Composites Part B: Engineering*, 36(2), 99-113.

Yuan, H., Teng, J. G., Seracino, R., Wu, Z. S. and Yao, J., (2004). "Full-range behavior of FRP-to-concrete bonded joints." *Engineering Structures*, 26(5), 553-565.

Zhang, D., Ueda, T. and Furuuchi, H., (2011). "Intermediate Crack Debonding of Polymer Cement Mortar Overlay-Strengthened RC Beam." *Journal of materials in civil engineering*, 23(6), 857-865.

APPENDIX

VITA

The author, Chanh Thai Minh Tran, was born on April 24th, 1982. His hometown is Tay Ninh province, Vietnam. He graduated his Bachelor of Civil Engineering degree from Hochiminh City University of Technology in 2005. After that, he worked at Hochiminh City University of Technology as assistant lecturer and continued to study Master degree of Civil Engineering at Hochiminh City University of Technology. He finished his Master degree in 2008. In 2010, he achieved the scholarship by the ASIAN University Network/Southeast Asia Engineering Education Development Network-AUN/SEED-Net (AUN/SEED-Net) for his doctoral degree of Civil Engineering at Chulalongkorn University, Bangkok, Thailand under the supervision of Associate Professor Dr. Boonchai Stimannaithum from Chulalongkorn University, Thailand and Professor Dr. Ueda Tamon from Hokkaido Universtiy, Japan.